NASA Technical Memorandum 83729

Application of Finite Element Substructuring to Composite Micromechanics

John J. Caruso
Lewis Research Center
Cleveland, Ohio

August 1984

NASA

TABLE OF CONTENTS

Page

LIST OF SYMBOLS

Symbols

C	heat capacity
D	diffusivity
E	modulus
G	shear modulus
K	thermal conductivity
k	volume ratio
A	thermal expansion coefficient
B	hygral (moisture) expansion coefficient
V	Poisson's ratio
p	density

Subscripts

f	fiber
L	ply
m	matrix
v	void

Direction

11	longitudinal

Direction	
22	transverse horizontal
33	transverse vertical
12	longitudinal shear
23	transverse shear

CHAPTER 1

INTRODUCTION

A variety of properties of unidirectional fiber composites are essential to the analysis/design of composite structures. These properties can be measured and/or predicted using theories with various levels of sophistication[1,2,3,4]. Recently, a simplified hygral-thermal-mechanical (HTM) composite micromechanics set of equations has been developed[5]. However, advanced finite element methods have not been used to predict hygral-thermal properties of unidirectional fiber composites. In addition, advanced finite element methods, such as hierarchical substructuring, have not been applied to fiber composite micromechanics. In models where a number of fibers are analyzed, the mesh repetition lends itself nicely to substructuring. Thus modeling advantages over the direct use of conventional elements are gained. The primary objective of this investigation, therefore, is to apply substructuring methods to fiber composite micromechanics. A secondary objective is to validate (numerically) the simplified, unified composite micromechanics theory[5].

The finite element (FE) method is used to predict the HTM properties of unidirectional composites. A three dimensional analysis

is performed on a model made of a single fiber with a square matrix material surrounding the fiber. The fiber matrix unit is considered a square array with depth (as explained latter). Another model made of nine cells is also used to predict the composite HTM properties. It is made of nine single fiber square array models using substructuring (superelement technique).

The single fiber square array model is investigated using conventional techniques. The model provides ease of analysis and a small unit of repetition for the superelement technique. The nine cell model contains eight superelement single cell models and one conventional single cell model. The nine cell model analysis is performed for two reasons. First, it determines whether FE substructuring can be used advantageously for fiber composite micromechanics. Second, accuracy of the single cell model's results are determined. Another nine cell model is generated using conventional techniques to check the superelement model results and to compare computer (CPU) time. It is also a check of the single cell model. This investigation uses two FE codes to perform the analysis of the models. COSMIC NASTRAN is used to perform analysis of a preliminary model. MSC/NASTRAN[6] is used to analyze the three models mentioned above.

The simplified micromechanics equations (SME) are used to compute composite properties for several composite systems. The SME are programmed in a computer code called UCPP (Unidirectional Composites Property Predictions). The program is used to compute all

the composite properties for each of the composite systems studied. The programmed SME predict the hygral, thermal and mechanical properties of a unidirectional composite.

The results from the FE codes are used to compute the HTM ply properties from fundamental mechanics of materials[7]. The mechanics of materials equations and the calculations to determine the HTM properties are shown in the Appendix for each specific model. This allows one to utilize this FE technique to compute HTM properties for assorted fiber and matrix combinations.

The properties predicted from the FE investigations are compared to those predicted by the SME. Confidence in the HTM properties predicted by the SME comes from these comparisons.

CHAPTER 2

THEORETICAL FUNDAMENTALS

2.1 Finite Element

The FE method subdivides a structure into a finite number of discrete elements. The FE code (MSC/NASTRAN) uses an isoparametric formulation of element geometry and displacement field. The three dimensional analysis allows three displacement degrees of freedom at each nodal point on the element.

The integration function is also determined by the element. The pentahedral and hexahedral elements use a Gauss Integration Scheme with two nodal points. Once the integration function is formed, it is used to derive the stiffness matrix for both elements.

MSC/NASTRAN is one of two FE codes used in this investigation. The CHEXA and CPENTA elements that form the MSC/NASTRAN library are used during this investigation. Both elements have an isoparametric formulation. The CHEXA and CPENTA elements allow MSC to utilize isotropic, orthotropic, and anisotropic materials in the analysis. MSC is performed on a Cray 1-S system. All results given in this report are MSC/NASTRAN generated. The other code used in the initial stages of this investigation is COSMIC NASTRAN. The CHEXA1 and CWEDGE elements only handle isotropic material. The program is run on a Univac 1100 system.

2.2 Composite Micromechanics

The composite SME for HTM properties provide a means of predicting properties without expensive analysis. The SME use fiber and matrix properties along with degrading effects, such as void formation and moisture entrapment during the fabrication process to predict these properties.

The composite SME follow assumptions that are based on physical conditions. The assumptions of major importance are: (1) the ply resists in-plane loads as shown in Figure 2.1; and (2) the ply and its constituents exhibit linear elastic behavior to fracture as is illustrated in Figure 2.2. With these assumptions and the use of mechanics of materials, the SME can be explicitly derived. The SME used in this study are summarized in Figures 2.3, 2.4 and 2.5 (Ref. 5).

2.3 Modeling and Validation

The FE model chosen for this research project is one generated during the preliminary stages of this investigation. The FE model consists of 125 nodal points and 96 elements. The 96 elements include 64 CHEXA1 and 32 CWEDGE (COSMIC NASTRAN). The CHEXA1 and CWEDGE are eight and six node linear three-dimensional brick elements (Fig. 2.6). Results from this preliminary investigation produce a good correlation between the mechanical and thermal properties for a metal matrix composite as predicted by FE analysis and the SME.

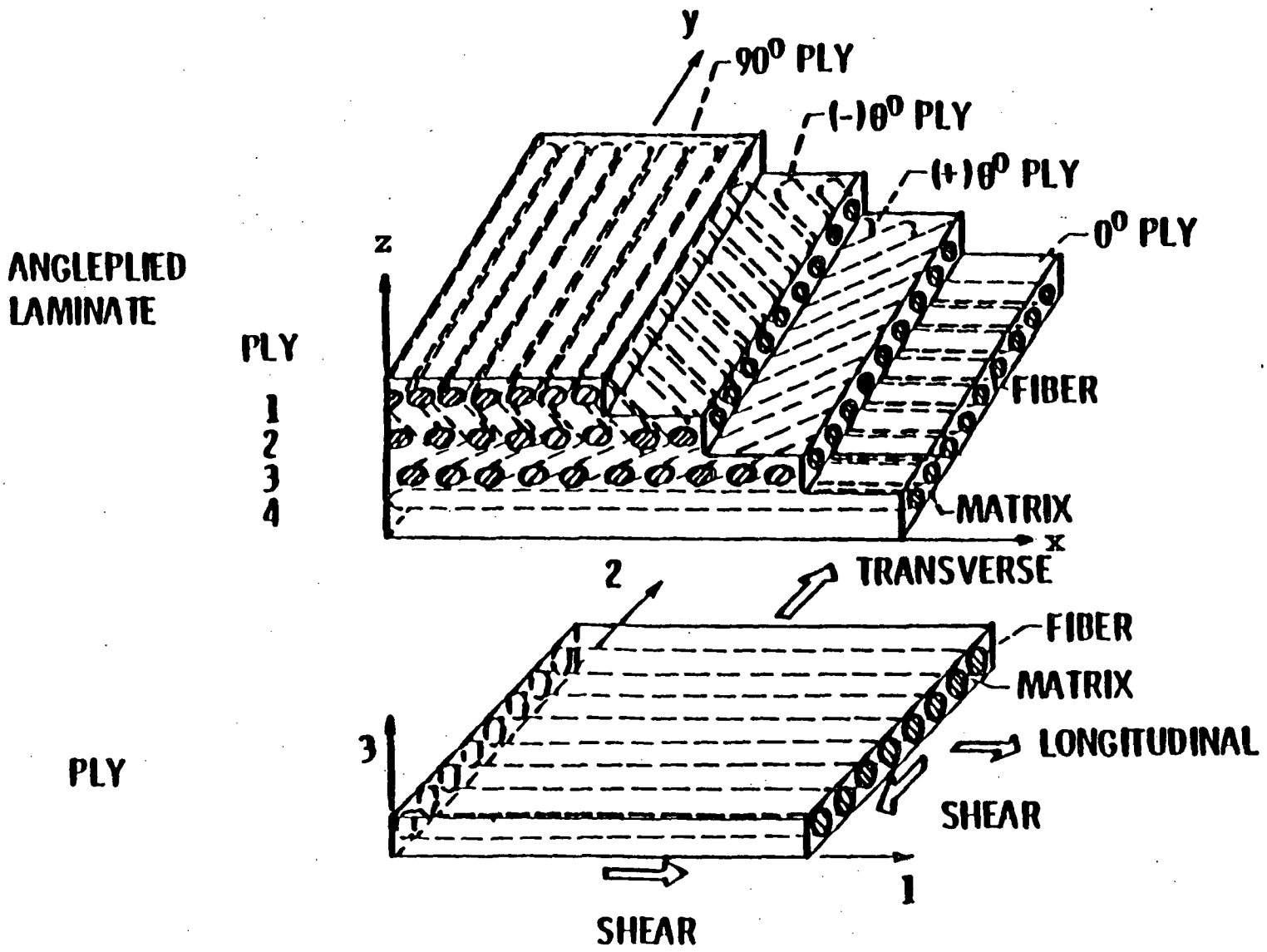

Figure 2.1 - Typical fiber composite geometry

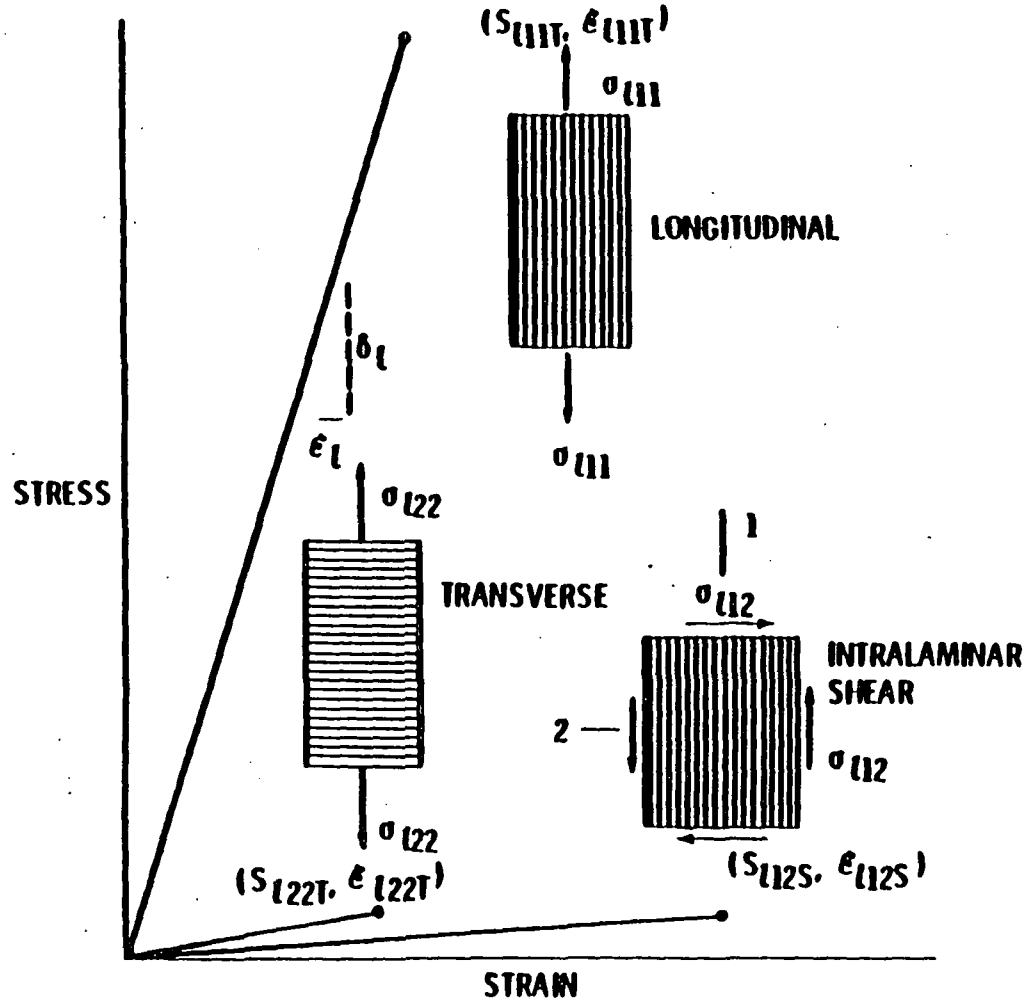

Figure 2.2 - Typical stress-strain behavior of unidirectional fiber

LONGITUDINAL MODULUS: $E_{\ell 11} = k_f E_{f11} + k_m E_m$

TRANSVERSE MODULUS: $E_{\ell 22} = \dfrac{E_m}{1 - \sqrt{k_f}\,(1 - E_m / E_{f22})} = E_{\ell 33}$

SHEAR MODULUS: $G_{\ell 12} = \dfrac{G_m}{1 - \sqrt{k_f}\,(1 - G_m / G_{f12})} = G_{\ell 13}$

SHEAR MODULUS: $G_{\ell 23} = \dfrac{G_m}{1 - k_f\,(1 - G_m / G_{f23})}$

POISSON'S RATIO: $\nu_{\ell 12} = k_f \nu_{f12} + k_m \nu_m = \nu_{\ell 13}$

POISSON'S RATIO: $\nu_{\ell 23} = \dfrac{E_{\ell 22}}{2G_{\ell 23}} - 1$

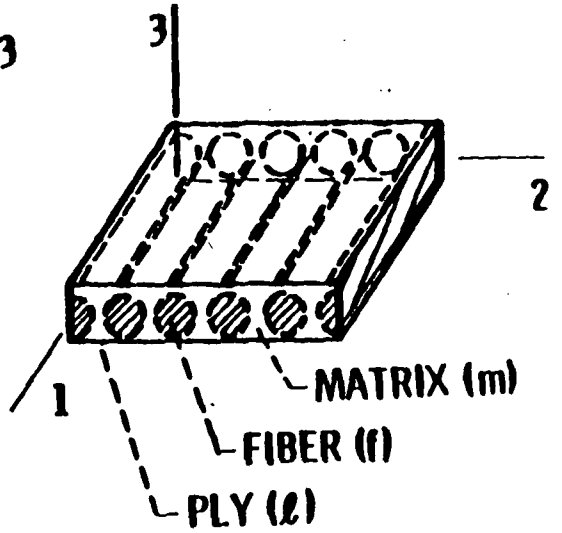

Figure 2.3 - Composite micromechanics mechanical properties

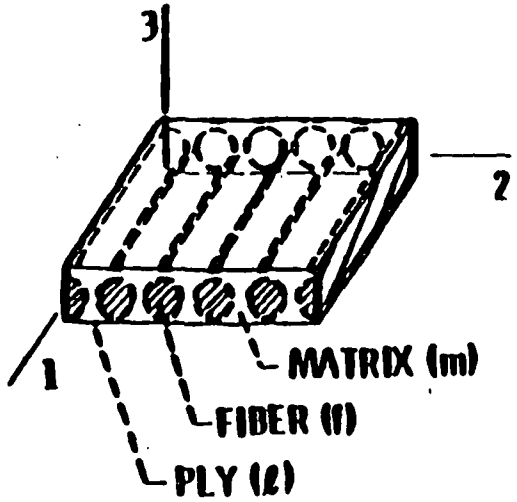

LONGITUDINAL CONDUCTIVITY: $K_{\ell 11} = k_f K_{f11} + k_m K_m$

TRANSVERSE CONDUCTIVITY: $K_{\ell 22} = (1 - \sqrt{k_f}) K_m + \dfrac{K_m \sqrt{k_f}}{1 - \sqrt{k_f}\,(1 - K_m / K_{f22})} = K_{\ell 33}$

LONGITUDINAL THERMAL EXPANSION COEFFICIENT: $\alpha_{\ell 11} = \dfrac{k_f \alpha_{f11} E_{f11} + k_m \alpha_m E_m}{E_{\ell 11}}$

TRANSVERSE THERMAL EXPANSION COEFFICIENT: $\alpha_{\ell 22} = \alpha_{f22} \sqrt{k_f} + (1 - \sqrt{k_f})(1 + k_f \nu_m E_{f11} / E_{\ell 11}) \alpha_m = \alpha_{\ell 33}$

Figure 2.4 - Composite micromechanics thermal properties

LONGITUDINAL DIFFUSIVITY $D_{\ell 11} = (1 - k_f) D_m$

TRANSVERSE DIFFUSIVITY $D_{\ell 22} = (1 - \sqrt{k_f}) D_m = D_{\ell 33}$

LONGITUDINAL MOISTURE EXP. COEF. $\beta_{\ell 11} = \beta_m (1 - k_f) E_m / E_{\ell 11}$

TRANSVERSE MOISTURE EXP. COEF. $\beta_{\ell 22} = \beta_m (1 - \sqrt{k_f}) \left[1 + \frac{\sqrt{k_f} (1 - \sqrt{k_f}) E_m}{\sqrt{k_f} E_{\ell 22} + (1 - \sqrt{k_f}) E_m} \right] - \beta_{\ell 33}$

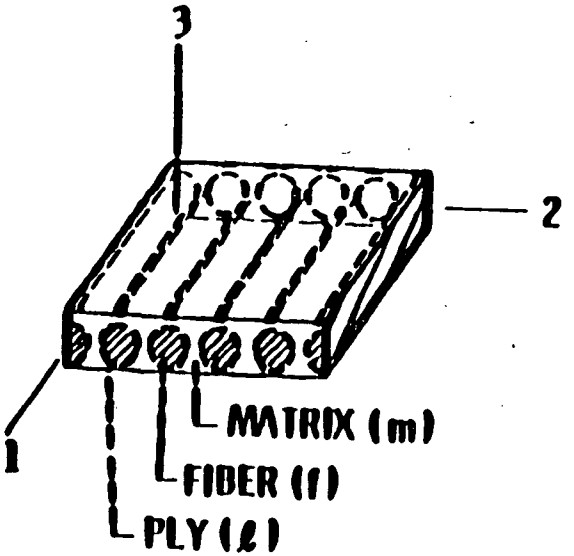

FOR INCOMPRESSIBLE MATRIX

$$\beta_{\ell 11} = 0$$

$$\beta_{\ell 22} = \beta_m \rho_\ell / 2\rho_m = \beta_{\ell 33}$$

Figure 2.5 - Composite micromechanics hygral properties

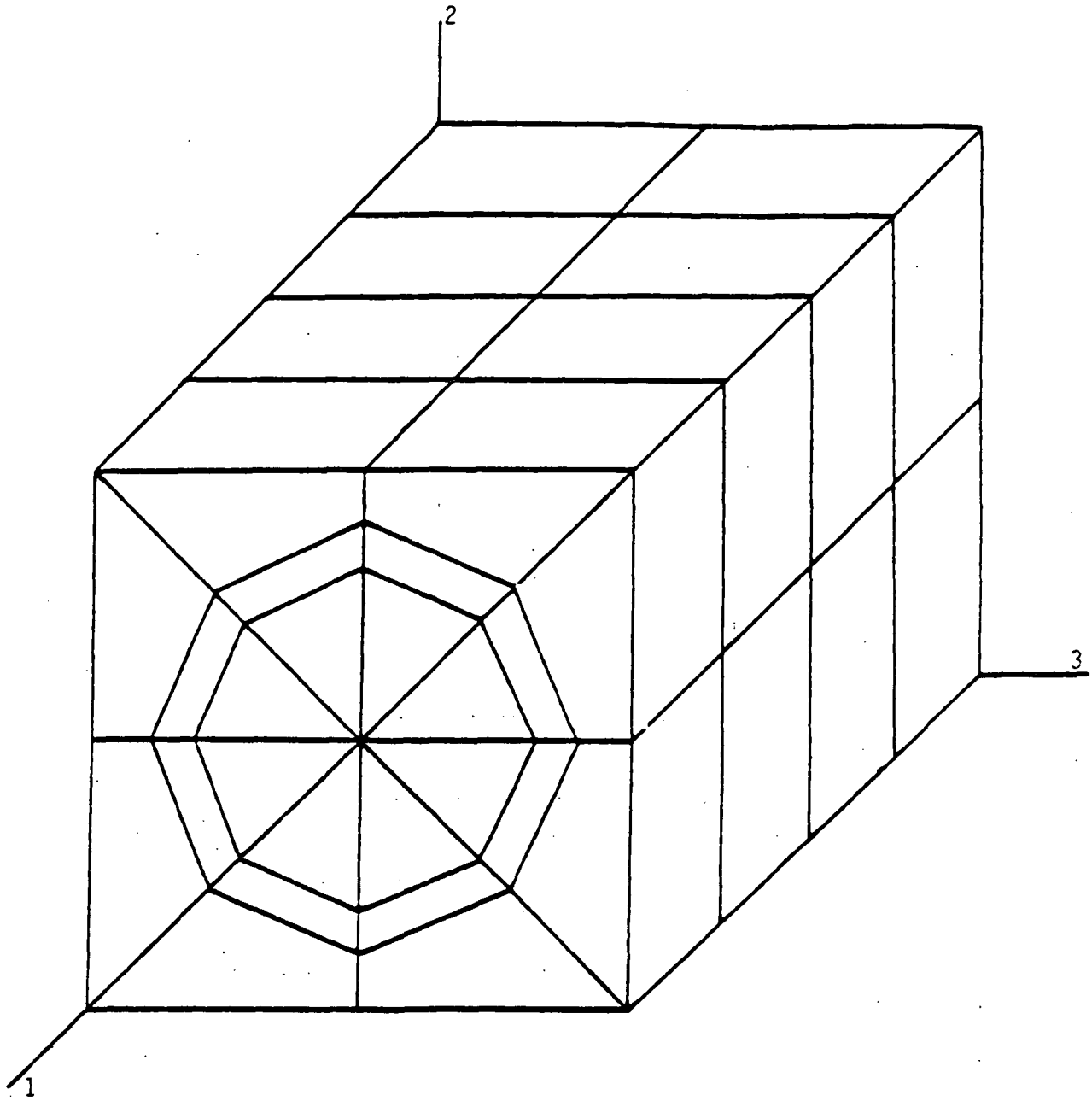

Figure 2.6 - Finite element model 125 node 96 element

The 125 node model is analyzed using COSMIC NASTRAN on a Univac 1100 system. The thermal and mechanical properties for a resin matrix composite, obtained from the FE model, do not compare well with the SME. Because of the poor results for the 125 node model, a second model is generated. For easy reference this new model will be called model 2 (M2). M2 has 245 nodal points and 192 elements (Fig 2.7). The element types are the same as those in the previous model.

M2 is analyzed using MSC/NASTRAN on a Cray 1-S system for various fiber/matrix modules ratios (EF/EM). The analyses provided a good comparison between the FE results and the SME. The results of this analysis are discussed in Chapter 3.

The change in FE codes from COSMIC to MSC/NASTRAN allows for the use of orthotropic material for the fiber and/or matrix. Since this investigation includes the analysis of a composite system with an orthotropic fiber, the elements have to be changed from CHEXA1 and CWEDGE to CHEXA and CPENTA, respectively. The new elements have the same characteristics as the old except as explained in section 2.1.

Model 3 (M3) has 245 nodal points and 192 elements. The 192 elements consists of 128 CHEXA and 64 CPENTA elements. The CHEXA and CPENTA are 8 and 6 node three-dimensional linear brick elements. The model has a single fiber in a square array of matrix material. This model is considered a single cell square array (Fig 2.7).

The investigation is continued using superelement analysis (MSC/NASTRAN rigid format 61). The superelement technique is chosen to include the neighboring fibers interaction in the model. To accomplish

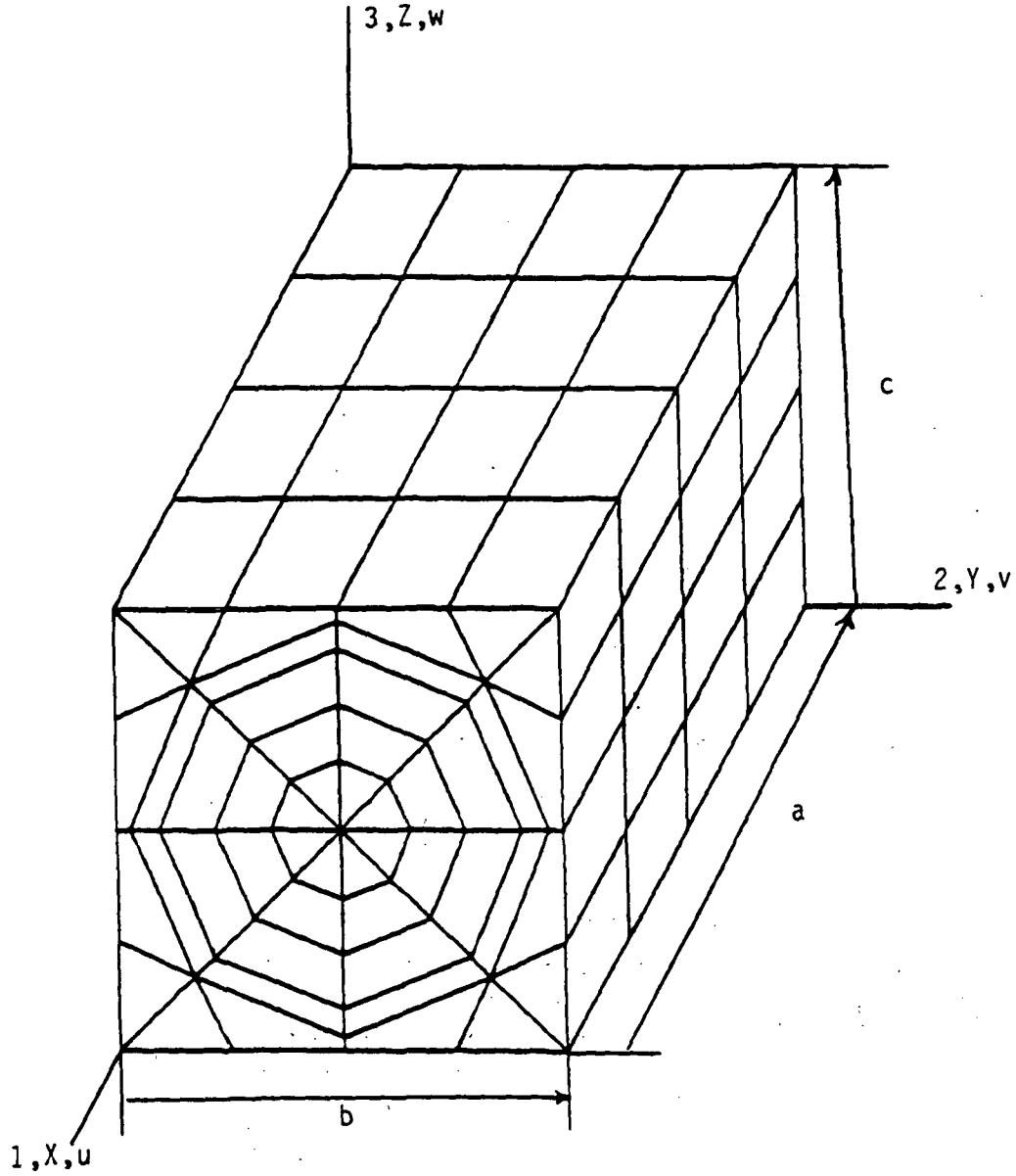

Figure 2.7 - Single cell model

this, a nine cell model is generated from the single cell model using image superelements with the same CHEXA and CPENTA elements used in the M3 analysis. The same elements are used to insure compatibility between the superelement model (Fig 2.8) and M3 (Fig 2.7).

The superelement model is analyzed using MSC/NASTRAN on a Cray 1-S computer system. The analysis of M3 and the superelement model are performed using the same boundary conditions corresponding to the property being determined. This is to guarantee the compatibility of the two models for comparison of the results.

The superelement model is compared to M3. M3 is analyzed on the Cray 1-S computer system in 5 to 9 seconds. The superelement model is also analyzed on the Cray 1-S computer system in 7 to 13 minutes. As can be seen, the time difference between the two models is very large. This large time difference between the M3 and superelement models leads to the generation of a conventional nine cell model to compare results and CPU time.

A nine cell model is generated using conventional techniques (without the use of superelements). The model consists of 1728 elements (Fig 2.9). The same CHEXA and CPENTA elements used in the two previous models are used in this model. The nine cell model is exactly the same as the superelement model used in the previous analysis except without the use of superelements. The new nine cell model will be considered model number five (M5). M5 is analyzed using MSC/NASTRAN on a Cray 1-S computer system with the same procedure used for the two previous analysis. The CPU time for M5 is 40 to 120 seconds.

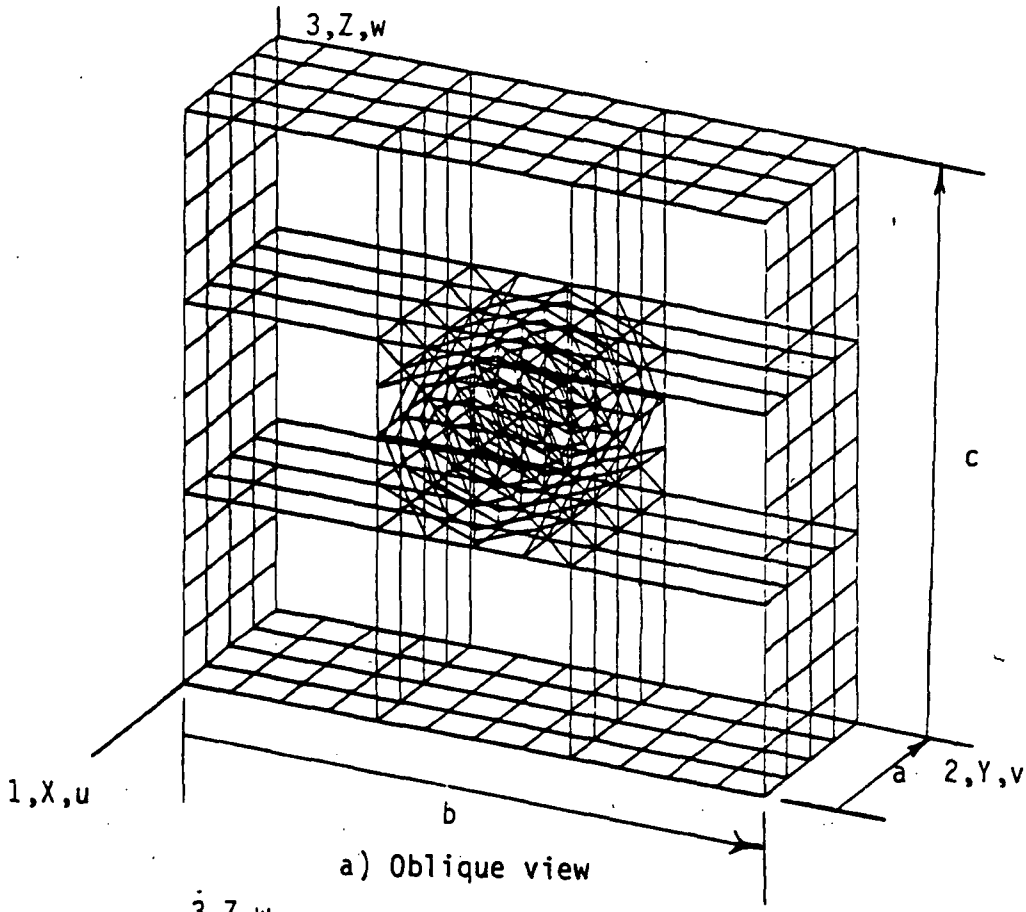

a) Oblique view

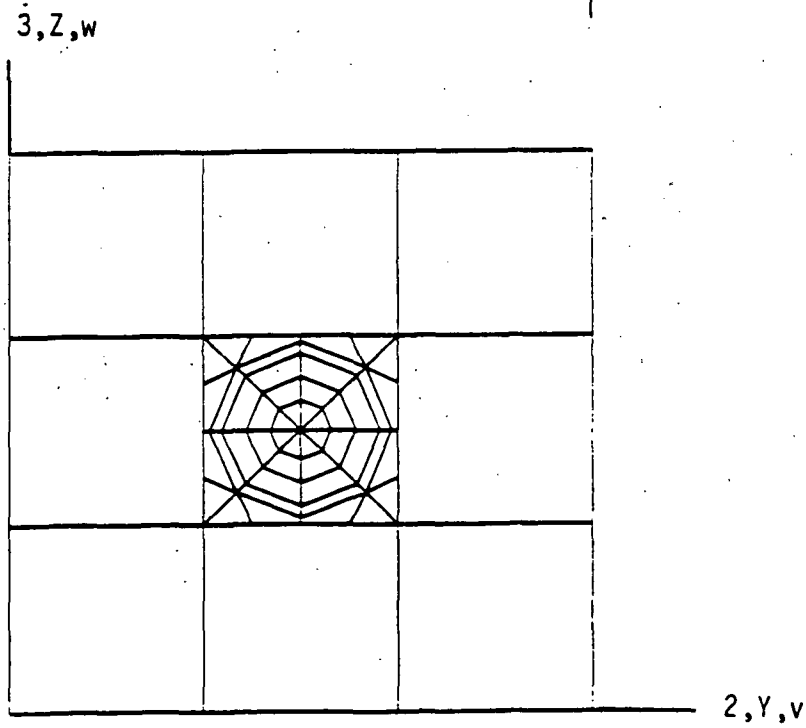

b) View looking down the longitudional axis

Figure 2.8 - Nine cell superelement model

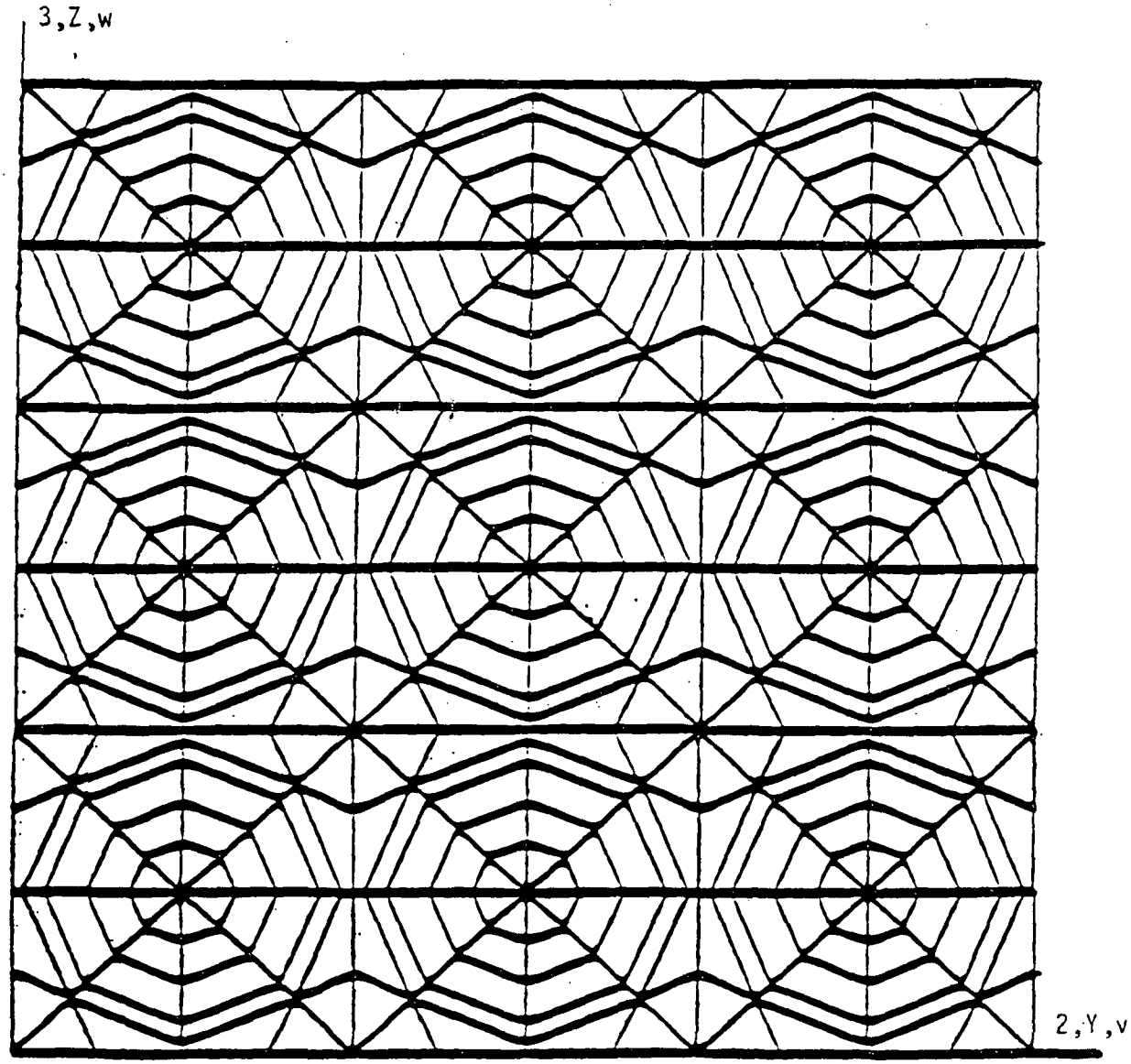

Figure 2.9 - Nine cell model

The difference in CPU time required to perform the analysis using the M5 model (Fig 2.9) versus the superelement model (Fig 2.8) is considerable. The large time involved in the superelement model rests on the number of exterior grid points. Since there are such a large number of external grid points, the CPU time used to analyze the model is large. The time involved in the use of superelements is not as important as being able to use the superelements telescopically to model a large number of individual fibers.

The superelement model may take considerably more time and produce the same results as M5; however, the superelement model can analyze a composite structure in much greater detail than conventional analysis. Therefore, the superelement technique can be used to model composite structures advantageously.

CHAPTER 3

RESULTS AND DISCUSSION

The micromechanics properties as predicted by the SME and the MSC/NASTRAN FE code are discussed in this chapter. The specific FE approach used to compute the composite properties is explained in the Appendix. The SME used to obtain the composite properties are described in Chapter 2.

3.1 Various Fiber/Matrix Modulus Ratios (EF/EM)

The investigation begins by analyzing the M2 model discussed in Chapter 2. The model is analyzed using MSC/NASTRAN on a Cray 1-S computer system. The analysis is performed to give mechanical and thermal properties for a range of fiber/matrix modulus ratios. The only fiber used in this portion of the analysis is boron. The matrix materials include titanium, aluminum, and two fictitious materials (Fict 1 and Fict 2). This permits the estimation of composite micromechanics properties for different composite systems. The properties of each system are determined as a function of fiber/matrix modulus ratios and fiber volume ratios.

The composite properties from the FE model M2 (Fig 2.7) analysis and the SME are shown in Table 3.3. This table should be used as a guide for initial comparison of the composite micromechanics properties. More accurate properties can be obtained from a complete investigation

TABLE 3.1

FIBER PROPERTIES

PROPERTY	SYMBOL	UNITS	FIBER		
			BORON	S-GLASS	AS
NUMBER OF FIBERS/ENDS	N_f	--	1.00	204	10000
FIBER DIAMETER	d_f	in.	0.0056	0.00036	0.0003
DENSITY	$_f$	lb/in^3	0.095	0.090	0.063
LONG. MODULUS	E_{f11}	Mpsi	58.0	12.4	31.0
TRANS. MODULUS	E_{f22}	Mpsi	58.0	12.4	2.00
LONG. SHEAR MODULUS	G_{f12}	Mpsi	24.2	5.17	2.00
TRANS. SHEAR MODULUS	G_{f23}	Mpsi	24.2	5.17	1.00
LONG. POISSON'S RATIO	V_{f12}	--	0.20	0.20	0.20
TRANS. POISSON'S RATIO	V_{f23}	--	0.20	0.20	0.25
HEAT CAPACITY	C_f	BTU/lb^oF	0.31	0.17	0.20
LONG. HEAT COND.	K_{f11}	$BTU\text{-}in/hr\text{-}^oF\text{-}ft^2$	22.0	21.0	580.
TRANS. HEAT COND.	K_{f22}	$BTU\text{-}in/hr\text{-}^oF\text{-}ft^2$	22.0	21.0	58.0
LONG. TH. EXP. COEF	A_{f11}	$10^{-6} in/in/^oF$	2.80	2.80	-0.55
TRANS. TH. EXP. COEF	A_{f22}	$10^{-6} in/in/^oF$	2.80	2.80	5.60
LONG. TENSILE STRENGTH	S_{ft}	ksi	600	600	350
LONG. COMPRESSION STR.	S_{fc}	ksi	700	--	350
SHEAR STRENGTH	S_{fs}	ksi	100	--	--

TABLE 3.2

MATRIX PROPERTIES

PROPERTY	SYMBOL	UNITS	MATRIX					
			HM	IMHS	FICT 1	TI	AL	FICT 2
DENSITY	ρ_m	lb/in^3	0.045	0.044	0.20	0.16	0.10	0.20
MODULUS	E_m	Mpsi	0.75	0.50	24.0	17.0	10.0	1.20
SHEAR MODULUS	G_m	Mpsi	--	--	9.23	6.54	3.85	0.462
POISSON'S RATIO	V_m	--	0.35	0.35	0.30	0.30	0.30	0.30
HEAT CAPACITY	C_m	$BTU/lb/^oF$	0.25	0.25	0.25	0.25	0.25	0.25
HEAT CONDUCTIVITY	K_m	$BTU/in/hr\text{-}ft^2\text{-}F^o$	1.25	1.25	1.25	1.25	1.25	1.25
THERMAL EXP. COEF.	A_m	$10^{-6}in/in/^oF$	40.0	36.0	24.0	40.0	12.0	24.0
DIFFUSIVITY	D_m	$10^{-10}in^2/sec$	0.60	0.60	0.60	0.60	0.60	0.60
MOISTURE EXP. COEF.	B_m	$10^{-2}in/in$	0.33	0.33	0.33	0.33	0.33	0.33
TENSILE STRENGTH	S_{mt}	ksi	20.0	15.0	--	--	--	--
COMPRESSION STRENGTH	S_{mc}	ksi	50.0	35.0	--	--	--	--
SHEAR STRENGTH	S_{ms}	ksi	15.0	13.0	--	--	--	--

NOTES: HM = High Modulus Epoxy; IMHS = Intermediate High Strength Epoxy; Fict 1 = Fictious Matrix; Titan = Titanimum; AL = Aluminum; Fict 2 = Fictitious Matrix

TABLE 3.3

THERMAL AND MECHANICAL PROPERTIES OF UNIDIRECTIONAL COMPOSITES

PROPERTY	UNITS	BORON/ FICT 1 SME	BORON/ FICT 1 M2	BORON/ TITANIUM SME	BORON/ TITANIUM M2	BORON/ ALUMINUM SME	BORON/ ALUMINUM M2	BORON/ FICT 2 SME	BORON/ FICT 2 M2
k_f		.466	.466	.466	.466	.466	.466	.466	.466
E_{L11}	Mpsi	39.8	39.9	36.1	36.1	32.4	32.4	27.7	27.7
E_{L22}	Mpsi	40.0	35.6	32.9	29.2	23.0	20.9	3.62	3.73
G_{L12}	Mpsi	16.0	14.2	13.0	11.5	9.04	8.16	1.40	1.37
G_{L23}	Mpsi	13.0	14.5	9.91	12.0	6.33	8.69	.851	1.58
V_{L12}		.253	.252	.253	.251	.253	.250	.253	.247
V_{L23}		.265	.281	.271	.292	.284	.306	.321	.337
A_{L11}	μ in/in^{o}F	9.62	10.2	3.10	3.13	4.23	4.55	3.29	3.71
A_{L22}	μ in/in^{o}F	9.97	15.2	3.23	3.50	6.24	8.20	11.4	15.4

NOTES: SME = Simplified Micromechanics Equations

M2 = Single Cell Finite Element Model Number two

using either the M3, superelement, or M5 models. The material properties used in the M2 analysis are summarized in Tables 3.1 and 3.2.

3.2 Micromechanics Properties

These properties are computed from two separate models and three different methods. Two of the methods for computing the properties are at two different sections of the nine cell model. Specifically, the properties are calculated using only the center cell of the nine cell model and all nine cells of the nine cell model. The M3 model will now be considered the single cell model (SC). The calculation using all nine cells is referred to as the multi-cell model (MC). The calculation using only the center cell of the multi-cell model is referred to as CCMC. The complete details (SC, MC, CCMC) of calculating the properties are discussed in the Appendix.

3.2.1 Mechanical Properties

The mechanical properties include Young's modulus, shear modulus, and Poisson's ratio. The properties are predicted for three composite systems; however, the boron/HM-epoxy system is discussed in much greater detail.

3.2.1.1. Longitudinal Modulus (E_{L11}). The analysis is performed by applying a uniform displacement field (u) to the surface (x=a) while the opposite surface (x=0) is fixed (Fig. 2.7). This method of analysis corresponds directly to the derivation of the composite SME

for the ply longitudinal modulus. The strain in the ply, fiber, and matrix are all equal. The longitudinal modulus and Poisson's ratio (V_{L12}), as predicted by the FE models, are consistent with the assumptions made in the derivation of the SME.

The comparisons between the SME and the FE predictions are shown in Table 3.4 for the three composite systems analyzed (boron/epoxy, s-glass/epoxy, AS/epoxy). It is noted in Table 3.4 that only the single cell FE analysis is necessary to predict the longitudinal modulus. Figure 3.1 indicates graphically how well the FE predictions agree with the SME. The three different FE models (Fig. 3.1) predict identical results.

3.2.1.2. Transverse Modulus (E_{L22}). The analysis is performed by applying a uniform displacement (v) to the surface (y=b) while the opposite surface (y=0) is fixed (Fig. 2.7). Applying displacement boundary conditions are not consistent with the assumptions made in the derivation of the SME for the ply transverse modulus; however, it avoids the steep stress gradients associated with the applied nodal point forces.

The comparisons between the SME and the FE predictions are shown in Figure 3.2 for the boron/HM-epoxy composite system. The FE predictions are in good agreement with that of the SME except for the values with 0.622 fiber volume ratio (k_f). The three different finite element models predict virtually identical results for k_f values less than 0.5 and start deviating slightly as k_f increases beyond 0.5.

TABLE 3.4

COMPARISON OF MODULI OF UNIDIRECTIONAL COMPOSITES

		BORON/HM-EPOXY Mpsi				S-GLASS/IMHS-EPOXY Mpsi				AS/IMHS-EPOXY Mpsi			
CALC.	k_f	E_{L11}	E_{L12}	G_{L12}	G_{L23}	E_{L11}	E_{L22}	G_{L12}	G_{L23}	E_{L11}	E_{L22}	G_{L12}	G_{L23}
SC	.622	36.4	4.35	1.35	1.49	7.89	2.44	.799	.868	19.5	1.21	.637	.500
MC		36.4	4.60	1.35	1.49	7.91	2.56	.797	.867	19.5	1.24	.827	.607
CCMC		36.6	4.60	1.35	1.49	8.08	2.56	.797	.867	19.7	1.24	.827	.607
SME		36.4	3.39	1.26	.722	7.90	2.06	.772	.462	19.5	1.22	.651	.375
SC	.466	27.4	2.31	.795	.921	6.05	1.42	.498	.565	14.7	.954	.438	.390
MC		27.4	2.44	.795	.921	6.05	1.49	.498	.566	14.7	.972	.601	.502
CCMC		27.7	2.44	.795	.921	6.22	1.49	.498	.566	14.9	.972	.601	.502
SME		27.4	2.30	.856	.515	6.05	1.45	.541	.336	14.7	1.02	.486	.298
SC	.224	13.5	1.20	.445	.523	3.16	.778	.290	.333	7.25	.677	.275	.272
MC		13.6	1.24	.446	.524	3.17	.799	.290	.334	7.35	.685	.398	.373
CCMC		13.8	1.24	.446	.524	3.33	.799	.290	.334	7.50	.685	.398	.373
SME		13.6	1.41	.522	.357	3.16	.915	.340	.236	7.32	.775	.324	.226
SC	.069	4.72	.875	.321	.349	1.32	.578	.212	.228	2.62	.555	.209	.211
MC		4.72	.876	.322	.350	1.33	.580	.208	.229	2.61	.556	.311	.307
CCMC		4.97	.876	.322	.350	1.49	.580	.208	.229	2.78	.556	.311	.307
SME		4.72	1.01	.376	.298	1.32	.669	.248	.198	2.61	.623	.243	.196

NOTES: SC = Single Cell; MC = Multi-Cell; CCMC = Center Cell of Multi-Cell;
SME = Simplified Micromechanics Equations

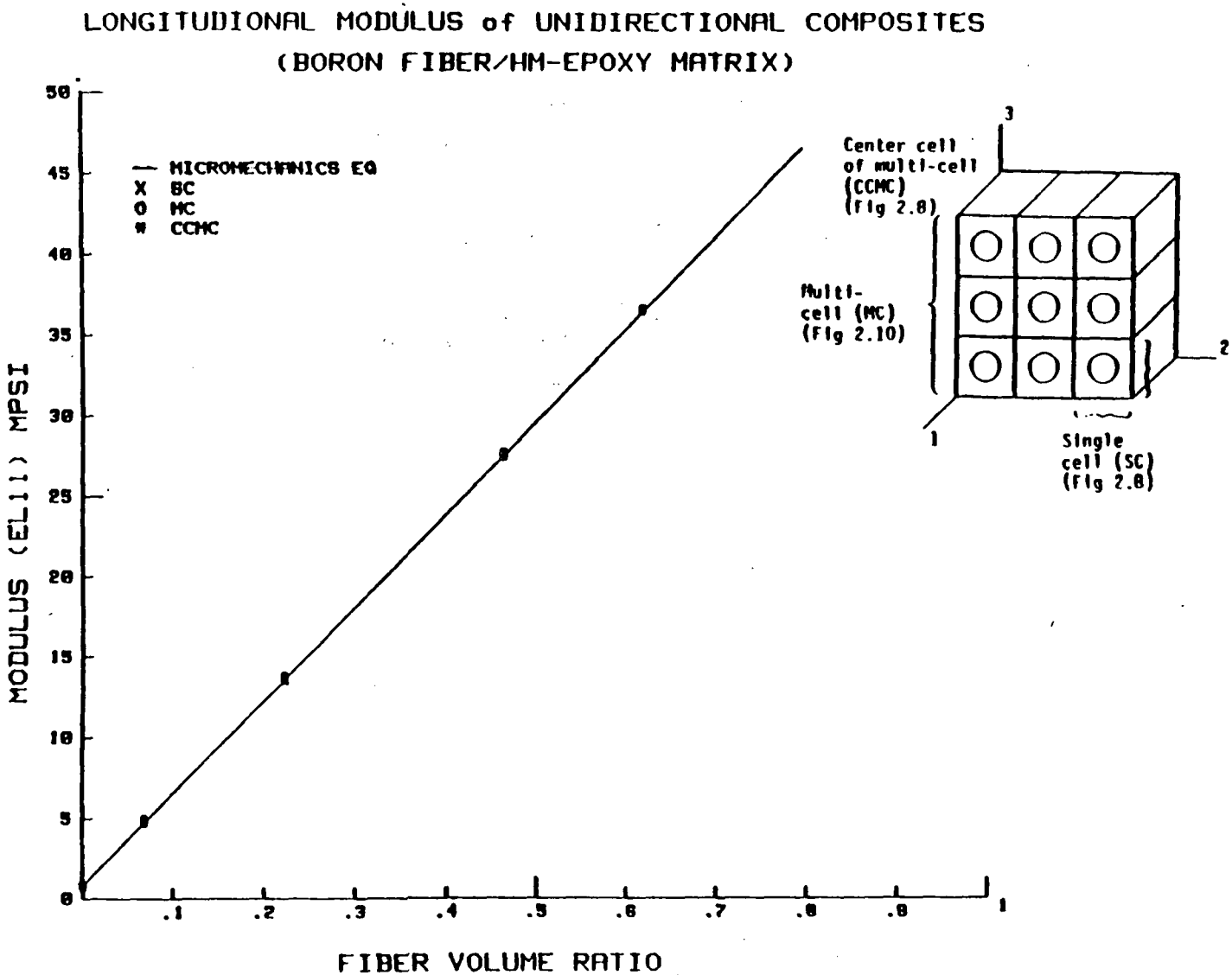
LONGITUDIONAL MODULUS of UNIDIRECTIONAL COMPOSITES
(BORON FIBER/HM-EPOXY MATRIX)
MICROMECHANICS EQ
X BC
O MC
* CCMC
MODULUS (EL11) MPSI
FIBER VOLUME RATIO
Center cell of multi-cell (CCMC) (Fig 2.8)
Multi-cell (MC) (Fig 2.10)
Single cell (SC) (Fig 2.8)
1
2
3

Figure 3.1

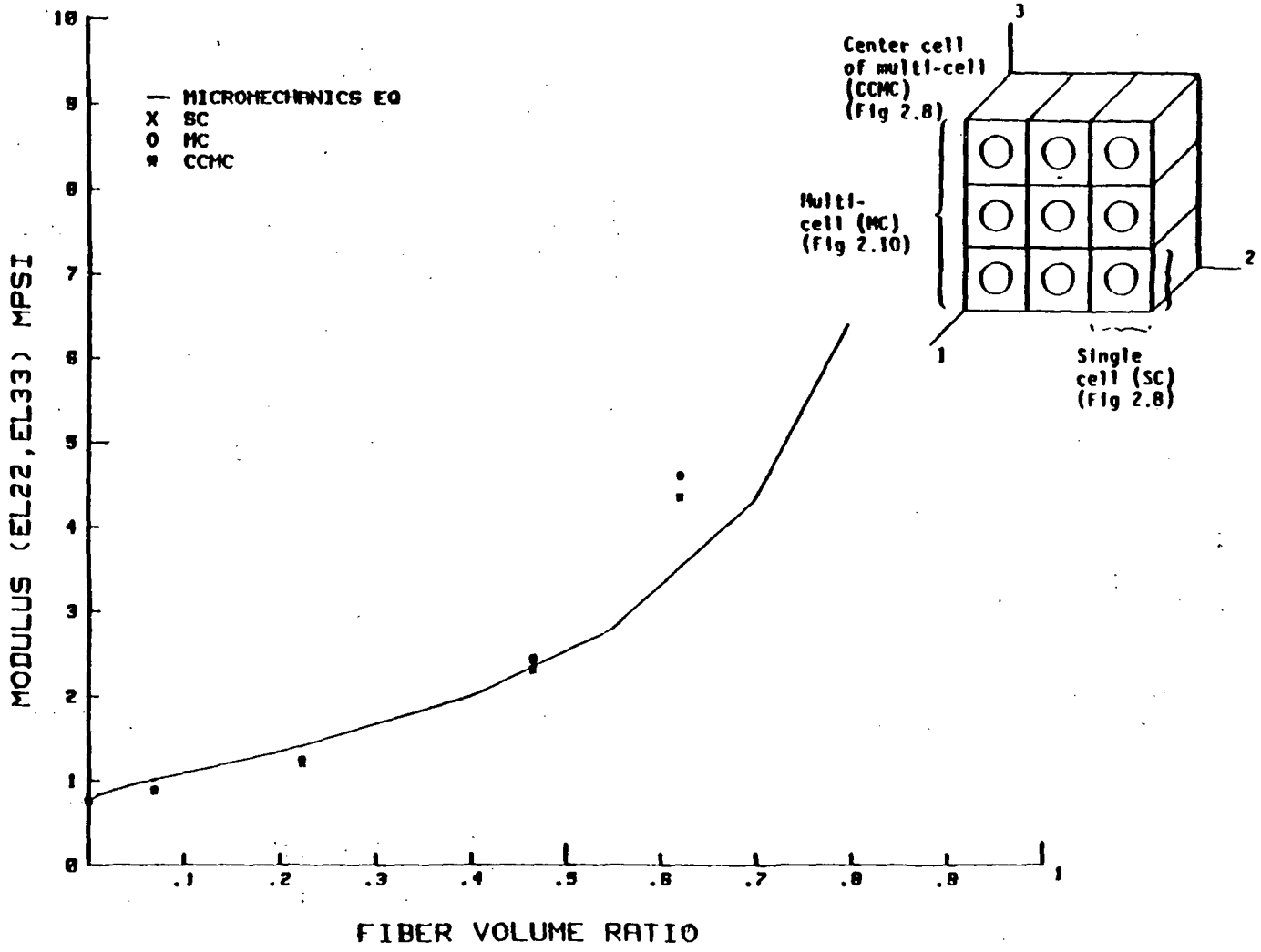
TRANSVERSE MODULUS of UNIDIRECTIONAL COMPOSITES
(BORON FIBER/HM-EPOXY MATRIX)
— MICROMECHANICS EQ
X SC
O MC
* CCMC
MODULUS (EL22,EL33) MPSI
FIBER VOLUME RATIO
Center cell of multi-cell (CCMC) (Fig 2.8)
Multi-cell (MC) (Fig 2.10)
Single cell (SC) (Fig 2.8)
1
2
3

Figure 3.2

The comparisons between the SME and the FE predictions for the three composite systems analyzed are summarized in Table 3.4.

3.2.1.3. Shear Modulus (G_{L12}). The analysis is performed by applying a uniform displacement (u) to the matrix on the surface (y=b) in the x-direction while the opposite surface (y=0) is fixed in the x-direction (Fig. 2.7). Also, the model is restrained from deforming along the y-direction in order to simulate simple shear.

The FE predictions do not agree with the SME prediction as well as originally expected as summarized in Table 3.4. However, the agreement is very good for the boron/HM-epoxy composite system as can be seen in Figure 3.3. The three different finite element models predict nearly identical results.

3.2.1.4. Shear Modulus (G_{L23}). The analysis is performed by applying a uniform displacement (w) to the matrix on the surface (y=b) in the z-direction while the opposite surface (y=0) is fixed in the z-direction (Fig. 2.7). No v-displacements are allowed in order to simulate simple shear.

The SME prediction is in very poor agreement with the FE predictions. The FE analysis seems to satisfy the same assumptions as in G_{L12}; however, the predicted results indicate otherwise as summarized in Table 3.4. It appears from the small amount of experimental results available that the SME predictions are more accurate than the FE predictions as shown in Figure 3.4. The

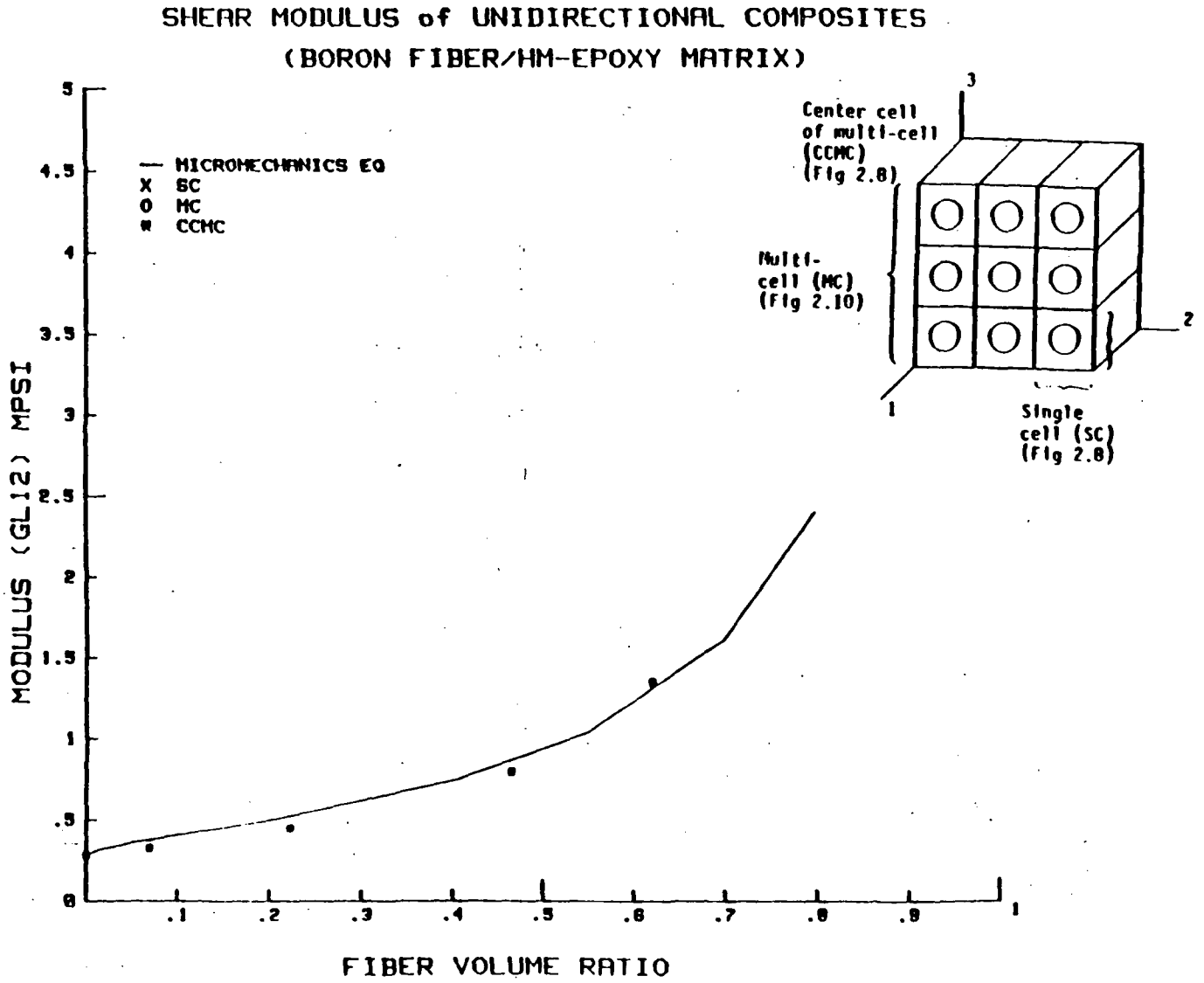
SHEAR MODULUS of UNIDIRECTIONAL COMPOSITES
(BORON FIBER/HM-EPOXY MATRIX)
— MICROMECHANICS EQ
X SC
O MC
* CCMC
MODULUS (GL12) MPSI
FIBER VOLUME RATIO
0
.5
1
1.5
2
2.5
3
3.5
4
4.5
5
.1
.2
.3
.4
.5
.6
.7
.8
.9
1
Center cell of multi-cell (CCMC) (Fig 2.8)
Multi-cell (MC) (Fig 2.10)
Single cell (SC) (Fig 2.8)
1
2
3

Figure 3.3

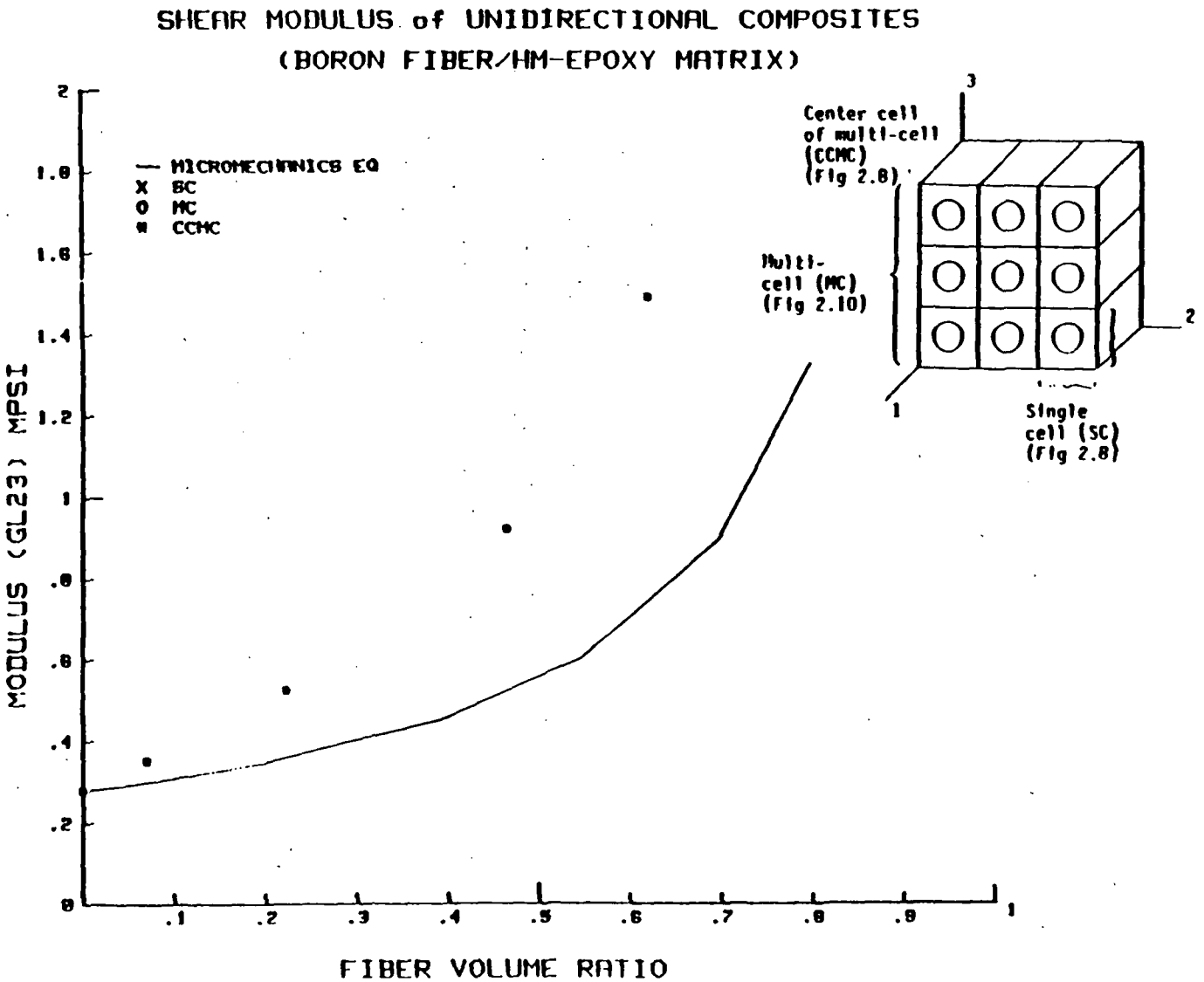
SHEAR MODULUS of UNIDIRECTIONAL COMPOSITES
(BORON FIBER/HM-EPOXY MATRIX)
— MICROMECHANICS EQ
X SC
O MC
■ CCMC
MODULUS (GL23) MPSI
FIBER VOLUME RATIO
Center cell of multi-cell (CCMC) (Fig 2.8)
Multi-cell (MC) (Fig 2.10)
Single cell (SC) (Fig 2.8)
1
2
3

Figure 3.4

reasons for this lack of agreement are discussed in Chapter 4. The predictions from the three different FE models are nearly identical.

3.2.1.5. Poisson's Ratio (V_{L12}). Poisson's ratio is computed from the same analysis as the longitudinal modulus.

The comparisons between the SME prediction and the FE predictions are shown in Figure 3.5 for the boron/HM-epoxy composite system. Table 3.5 contains the values of the Poisson's ratio for the three composite systems analyzed. The SME prediction and those from the three FE models are almost identical.

3.2.1.6. Poisson's Ratio (V_{L23}). Poisson's ratio is computed from the transverse modulus analysis described earlier(pg. 24).

The comparisons between the SME prediction and the FE results are shown in Figure 3.6 for the boron/HM-epoxy composite system. The MC analysis accounts for the interaction of the neighboring fibers as previously mentioned. That is the MC model acts more like a ply than does the SC model. For this reason, the predictions from the MC model are considered more accurate. The results for the three composite systems are summarized in Table 3.5 for Poisson's ratio (V_{L23}). As can be seen, the results predicted are considerably different for each of the different methods. This considerable difference is thought to be caused in part by the local Poisson-effect gradient through-the-thickness.

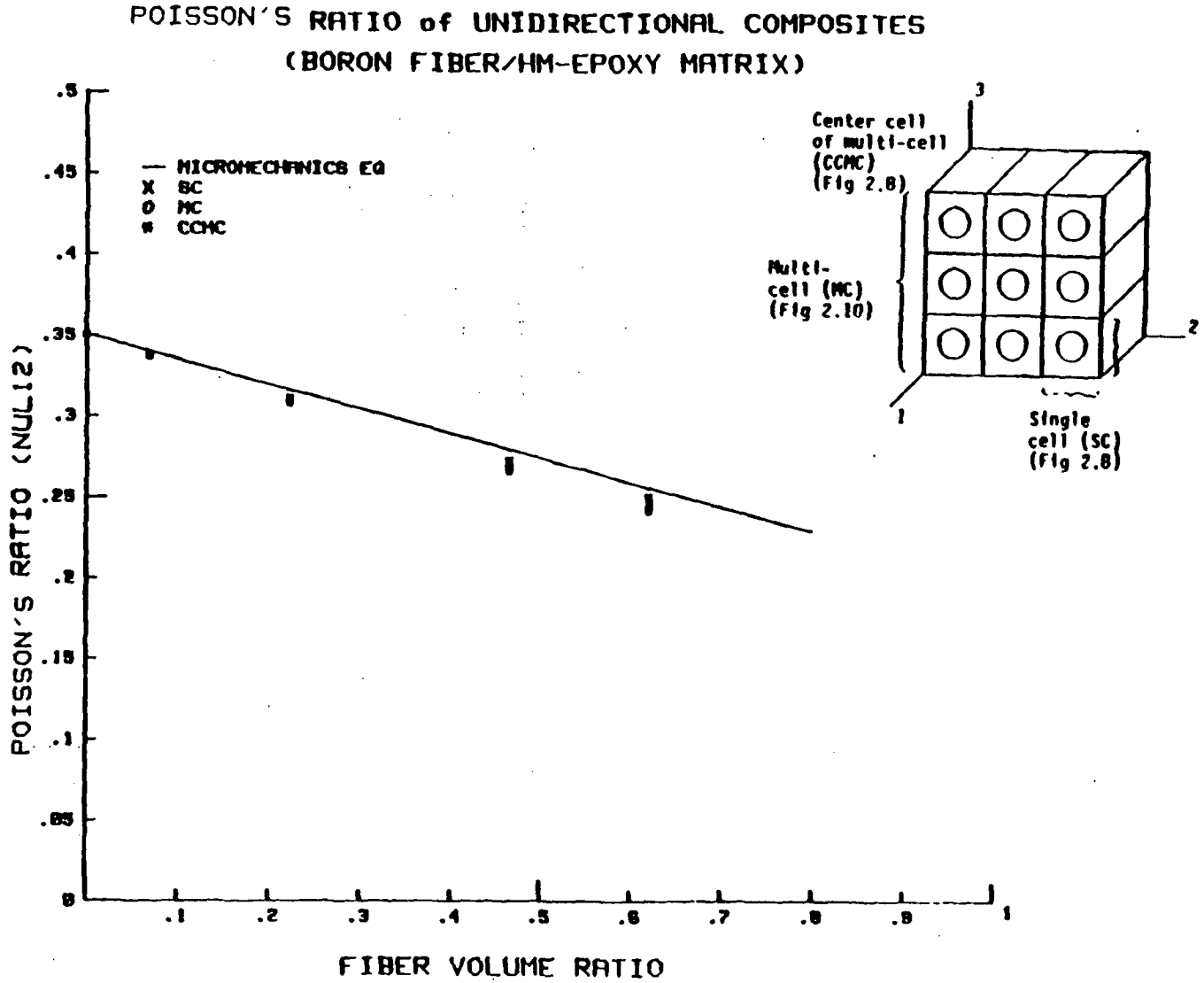
POISSON'S RATIO of UNIDIRECTIONAL COMPOSITES
(BORON FIBER/HM-EPOXY MATRIX)
— MICROMECHANICS EQ
X BC
O MC
* CCMC
Center cell of multi-cell (CCMC) (Fig 2.8)
Multi-cell (MC) (Fig 2.10)
Single cell (SC) (Fig 2.8)
1
2
3
POISSON'S RATIO (NU12)
FIBER VOLUME RATIO
.5
.45
.4
.35
.3
.25
.2
.15
.1
.05
0
.1
.2
.3
.4
.5
.6
.7
.8
.9
1

Figure 3.5

TABLE 3.5

COMPARISON OF POISSON'S RATIO OF UNIDIRECTIONAL COMPOSITES

CALC.	k_f	BORON/HM-EPOXY		S-GLASS/IMHS-EPOXY		AS/IMHS-EPOXY	
		V_{L12}	V_{L23}	V_{L12}	V_{L23}	V_{L12}	V_{L23}
SC	.622	.251	.413	.337	.375	.255	.374
MC		.245	.212	.337	.358	.251	.317
CCME		.242	.153	.336	.366	.249	.305
SME		.257	.340	.340	.400	.257	.374
SC	.466	.273	.467	.311	.408	.278	.396
MC		.269	.296	.310	.355	.275	.345
CCME		.267	.251	.310	.171	.274	.334
SME		.280	.372	.316	.398	.280	.396
SC	.224	.311	.417	.273	.430	.314	.394
MC		.309	.359	.270	.296	.313	.371
CCME		.308	.345	.270	.259	.313	.367
SME		.316	.417	.280	.359	.316	.428
SC	.069	.337	.380	.251	.391	.338	.374
MC		.337	.372	.246	.228	.338	.371
CCMC		.337	.370	.246	.091	.338	.373
SME		.340	.434	.257	.329	.340	.434

NOTES: SC = Single Cell; MC = Multi-Cell; CCMC = Center Cell of Multi-Cell;
SME = Simplified Micromechanics Equations

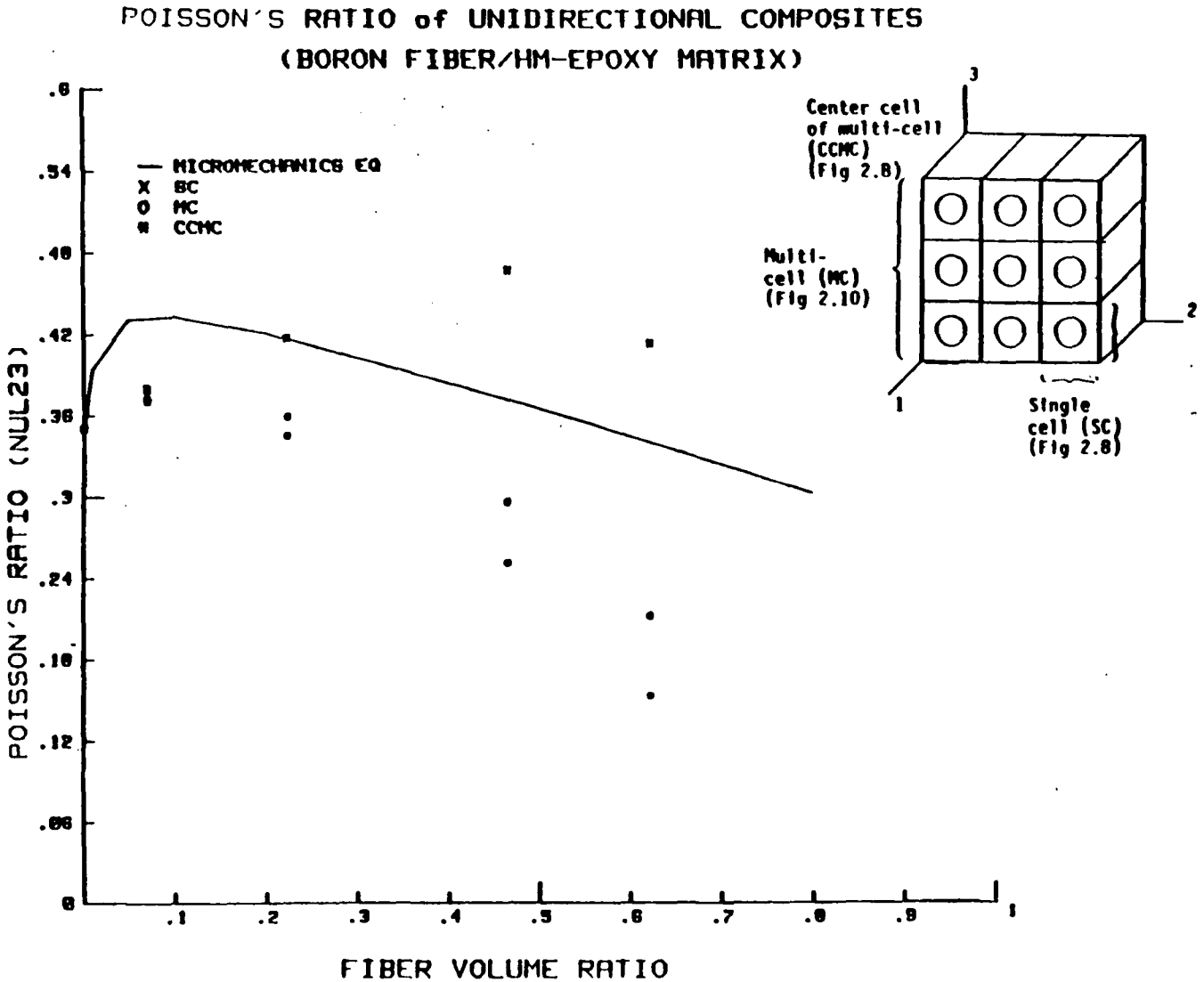
POISSON'S RATIO of UNIDIRECTIONAL COMPOSITES
(BORON FIBER/HM-EPOXY MATRIX)
— MICROMECHANICS EQ
X BC
O MC
* CCMC
Center cell of multi-cell (CCMC) (Fig 2.8)
Multi-cell (MC) (Fig 2.10)
Single cell (SC) (Fig 2.8)
1
2
3
POISSON'S RATIO (NU23)
FIBER VOLUME RATIO
0
.06
.12
.18
.24
.3
.36
.42
.48
.54
.6
.1
.2
.3
.4
.5
.6
.7
.8
.9
1

Figure 3.6

3.2.2 Thermal Properties

The thermal properties include the thermal expansion coefficients and the thermal conductivities. This section will also concentrate on boron/HM-epoxy system; however, the remaining two systems are included in the tables.

3.2.2.1. Longitudinal Coefficient of Expansion (A_{L11}). The analysis for the thermal expansion coefficient (TEC) is performed by applying a uniform temperature to the composite. The center plane of the structure in the longitudinal direction is fixed in the x-direction. The center planes of the structure in the y- and z- transverse directions are fixed in the y- and z- directions. Since the center planes are fixed in their respective directions, the composite is forced to deform symmetrically about these planes.

The comparison for the boron/HM-epoxy composite system is shown in Figure 3.7. The results from the three composite systems analyzed are summarized in Table 3.6. The results obtained from the FE analysis do not compare well with the SME predictions for longitudinal TEC. This poor correlation is attributed in part to the Poisson's restraining effect of the transverse TEC. The comparisons of the predicted results from the three FE analyses are almost identical.

3.2.2.2. Transverse Coefficient of Expansion (A_{L22}). The transverse thermal expansion coefficient (TEC) is computed from the same analysis as the longitudinal TEC.

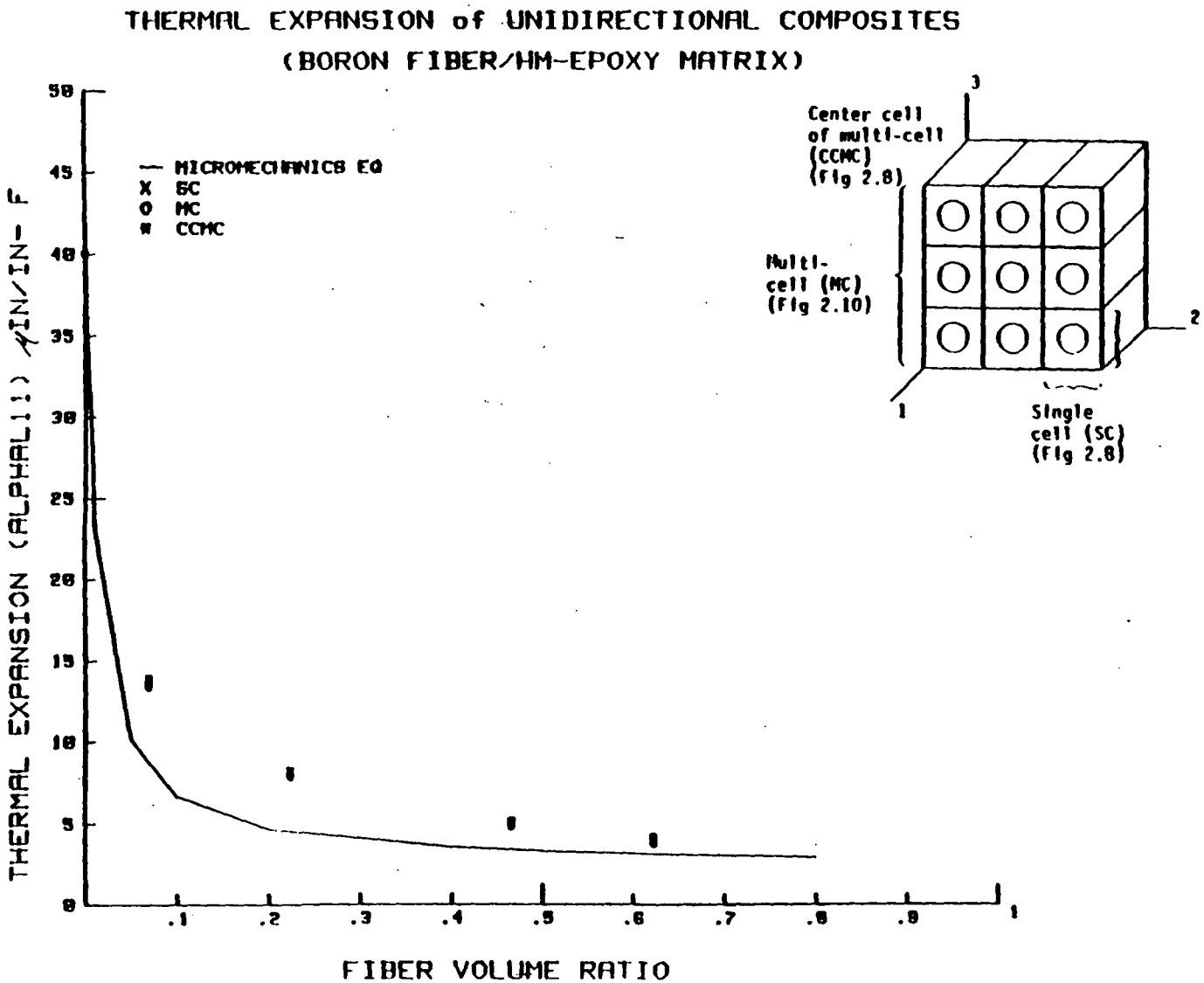
THERMAL EXPANSION of UNIDIRECTIONAL COMPOSITES
(BORON FIBER/HM-EPOXY MATRIX)
— MICROMECHANICS EQ
X SC
O MC
* CCMC
THERMAL EXPANSION (ALPHA11) μIN/IN- F
FIBER VOLUME RATIO
Center cell of multi-cell (CCMC) (Fig 2.8)
Multi-cell (MC) (Fig 2.10)
Single cell (SC) (Fig 2.8)
1
2
3

Figure 3.7

TABLE 3.6

COMPARISON OF THERMAL PROPERTIES OF UNIDIRECTIONAL COMPOSITES

CALC.	k_f	BORON/HM-EPOXY u in/in^{o}F				S-GLASS/IMHS-EPOXY u in/in^{o}F				AS/IMHS-EPOXY u in/in^{o}F			
		A_{L11}	A_{L22}	K_{L11}	K_{L22}	A_{L11}	A_{L22}	K_{L11}	K_{L22}	A_{L11}	A_{L22}	K_{L11}	K_{L22}
SC	.622	3.93	19.4	14.0	4.41	4.42	17.6	13.6	4.37	.778	20.8	365	5.03
MC		3.73	17.8	14.2	4.80	4.26	16.1	13.5	4.74	.500	19.8	367	5.57
CCMC		4.16	16.6	--	--	4.62	15.3	--	--	.844	19.4	--	--
SME		3.09	13.3	14.2	4.11	3.59	12.1	13.5	4.08	-.195	14.6	361	4.58
SC	.466	5.09	26.2	10.9	3.05	5.86	23.6	10.4	3.03	1.97	26.6	266	3.31
MC		4.75	25.2	10.9	3.16	5.59	22.7	10.5	3.15	1.61	26.0	268	3.44
CCMC		5.12	24.7	--	--	5.86	22.2	--	--	1.93	25.8	--	--
SME		3.34	18.6	10.9	2.79	4.27	16.7	10.4	2.78	.113	19.1	271	2.97
SC	.224	8.23	37.3	5.90	1.89	10.0	33.1	5.69	1.89	5.30	35.6	131	1.96
MC		7.83	37.0	5.89	1.91	9.66	32.7	5.66	1.91	4.88	35.5	130	1.98
CCMC		7.89	36.9	--	--	9.66	32.7	--	--	4.92	35.6	--	--
SME		4.40	28.8	5.89	1.73	6.88	25.3	5.67	1.72	1.39	27.8	131	1.76
SC	.069	13.9	43.9	2.68	1.42	17.8	38.0	2.62	1.42	11.4	40.4	41.1	1.44
MC		13.6	43.9	2.69	1.43	17.6	38.0	2.62	1.42	11.1	40.4	41.5	1.44
CCMC		13.3	44.1	--	--	17.3	38.2	--	--	10.7	40.7	--	--
SME		8.30	38.1	2.69	1.36	14.5	32.2	2.62	1.36	5.96	35.4	41.4	1.36

NOTES: SC = Single Cell; MC = Multi-Cell; CCMC = Center Cell of Multi-Cell;
SME = Simplified Micromechanics Equations

The predictions from the three FE models are collectively in poor agreement with those from the SME. The comparison for the boron/HM-epoxy composite system is shown in Figure 3.8. The results for the three composite systems are summarized in Table 3.6. The reasons for the differences among the different predictions are thought to be the same as those for V_{L23} and A_{L11}.

3.2.2.3. Longitudinal Thermal Conductivity (K_{L11}). This analysis is performed by applying a uniform temperature on the fiber matrix surface (x=a) Fig. 2.7. The air temperature at the opposite surface (x=0) is considerably lower than that applied to the composite. This allows heat to flow longitudinally through the structure. The side surfaces (y=0, b and z=0,c) are insulated so that no heat can escape through these surfaces. These surfaces are insulated to simulate the assumptions made in the derivation of the SME.

The predictions from the three FE models are identical and collectively compare well with the SME prediction as shown in Figure 3.9 for the boron/HM-epoxy composite system. The comparisons for the three composite systems analyzed are summarized in Table 3.6.

3.2.2.4. Transverse Thermal Conductivity (K_{L22}). This analysis is performed by applying a uniform temperature on the matrix surface (y=b) Fig. 2.7. The air temperature at the opposite surface (y=0) is lower than that applied to the structure. This allows heat to flow transversely through the structure. The remaining four surfaces are

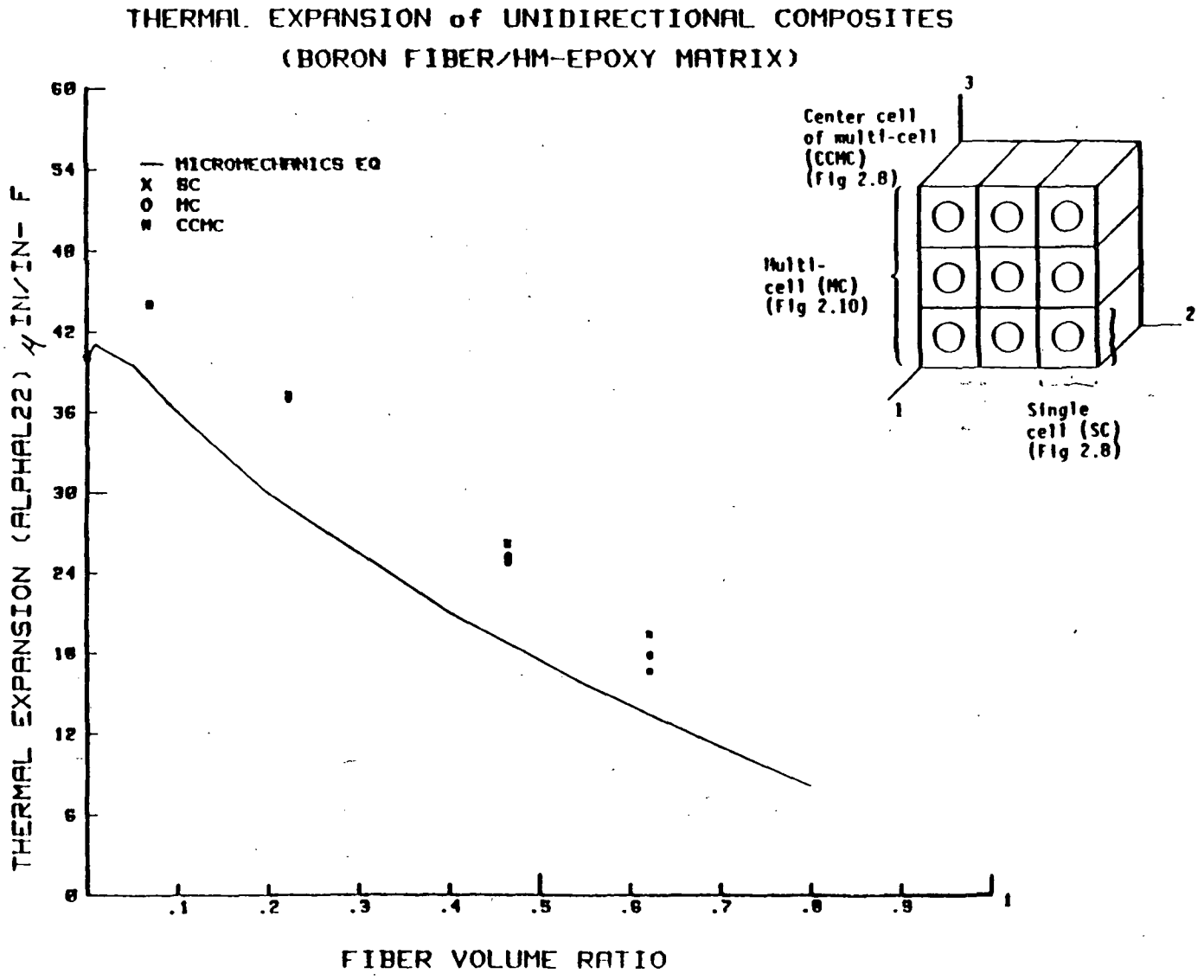
THERMAL EXPANSION of UNIDIRECTIONAL COMPOSITES
(BORON FIBER/HM-EPOXY MATRIX)
THERMAL EXPANSION (ALPHAL22) μIN/IN- F
MICROMECHANICS EQ
X SC
O MC
* CCMC
60
54
48
42
36
30
24
18
12
6
0
.1
.2
.3
.4
.5
.6
.7
.8
.9
1
FIBER VOLUME RATIO
3
2
1
Center cell of multi-cell (CCMC) (Fig 2.8)
Multi-cell (MC) (Fig 2.10)
Single cell (SC) (Fig 2.8)

Figure 3.8

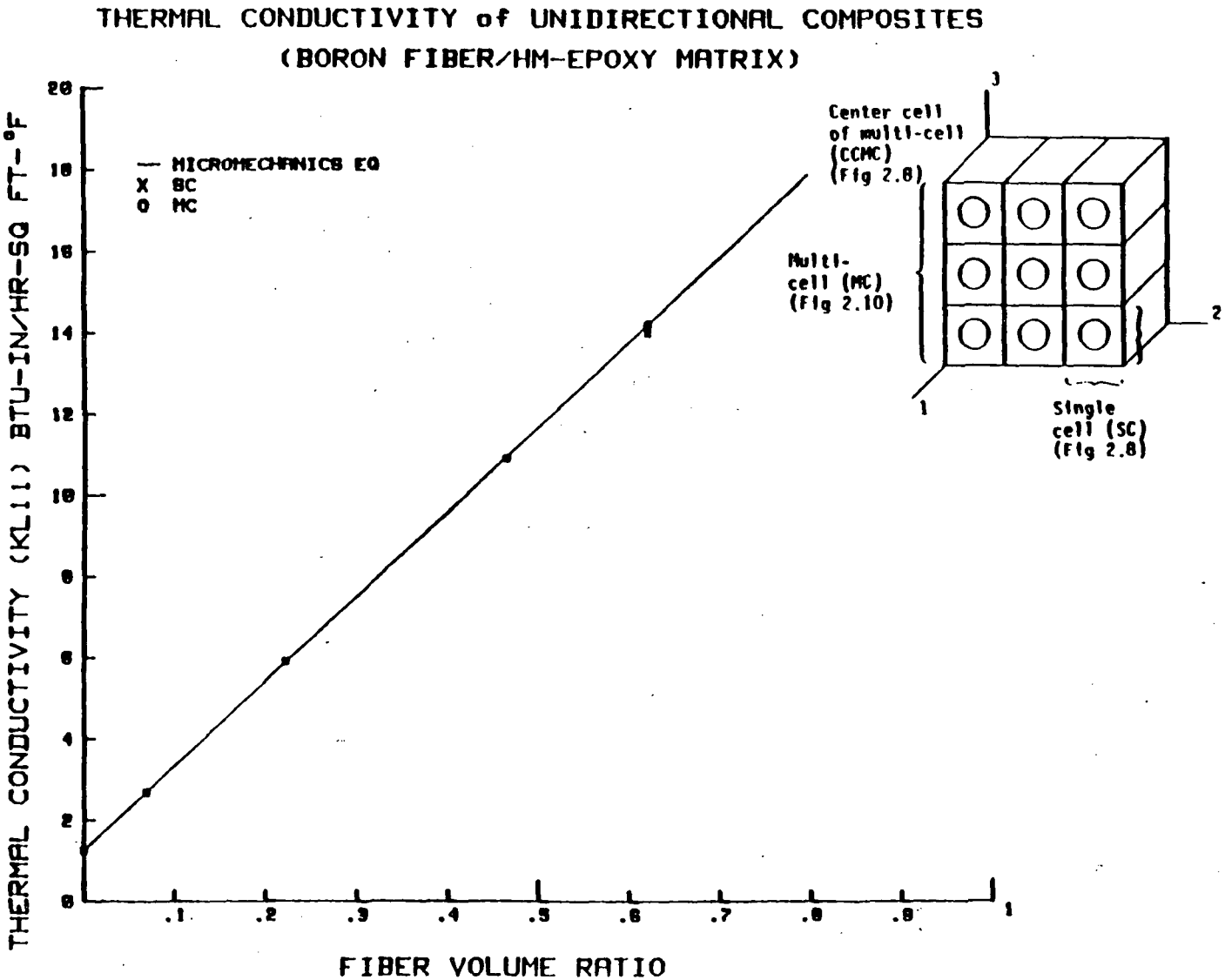
THERMAL CONDUCTIVITY of UNIDIRECTIONAL COMPOSITES
(BORON FIBER/HM-EPOXY MATRIX)
THERMAL CONDUCTIVITY (KL11) BTU-IN/HR-SQ FT-°F
FIBER VOLUME RATIO
— MICROMECHANICS EQ
X SC
o MC
Center cell of multi-cell (CCMC) (Fig 2.8)
Multi-cell (MC) (Fig 2.10)
Single cell (SC) (Fig 2.8)
1
2
3

Figure 3.9

insulated so that no heat can escape into the atmosphere. This is in agreement with assumptions made in the derivation of the SME.

The correlations between the SME prediction and those from the FE model predictions are reasonably good. The agreement becomes better with decreasing fiber volume ratio. The comparisons for the boron/HM-epoxy composite system are shown in Figure 3.10. The comparisons for the three composite systems analyzed are summarized in Table 3.6.

3.2.3 Hygral (Moisture) Properties

The hygral properties include the hygral expansion coefficients and the diffusivities. These properties are discussed in great detail for boron/HM-epoxy. The property predictions for the s-glass/IMHS-epoxy and the AS/IMHS-epoxy are also included.

3.2.3.1. Longitudinal Hygral Coefficient of Expansion (B_{L11}). The procedure used to determine the longitudinal hygral expansion coefficient (HEC) is the same as that described for the longitudinal TEC except that the HEC for the fiber is assumed to be zero.

The longitudinal HEC predicted from the SME is in poor agreement with those from the FE analysis as shown in Figure 3.11 for the boron/HM-epoxy composite system. Each of the three FE models provides nearly identical results. The comparisons for the three composite systems analyzed are summarized in Table 3.7. The same factors influencing the SME predictions for A_{L11} are thought to contribute to the poor agreement for B_{L11}.

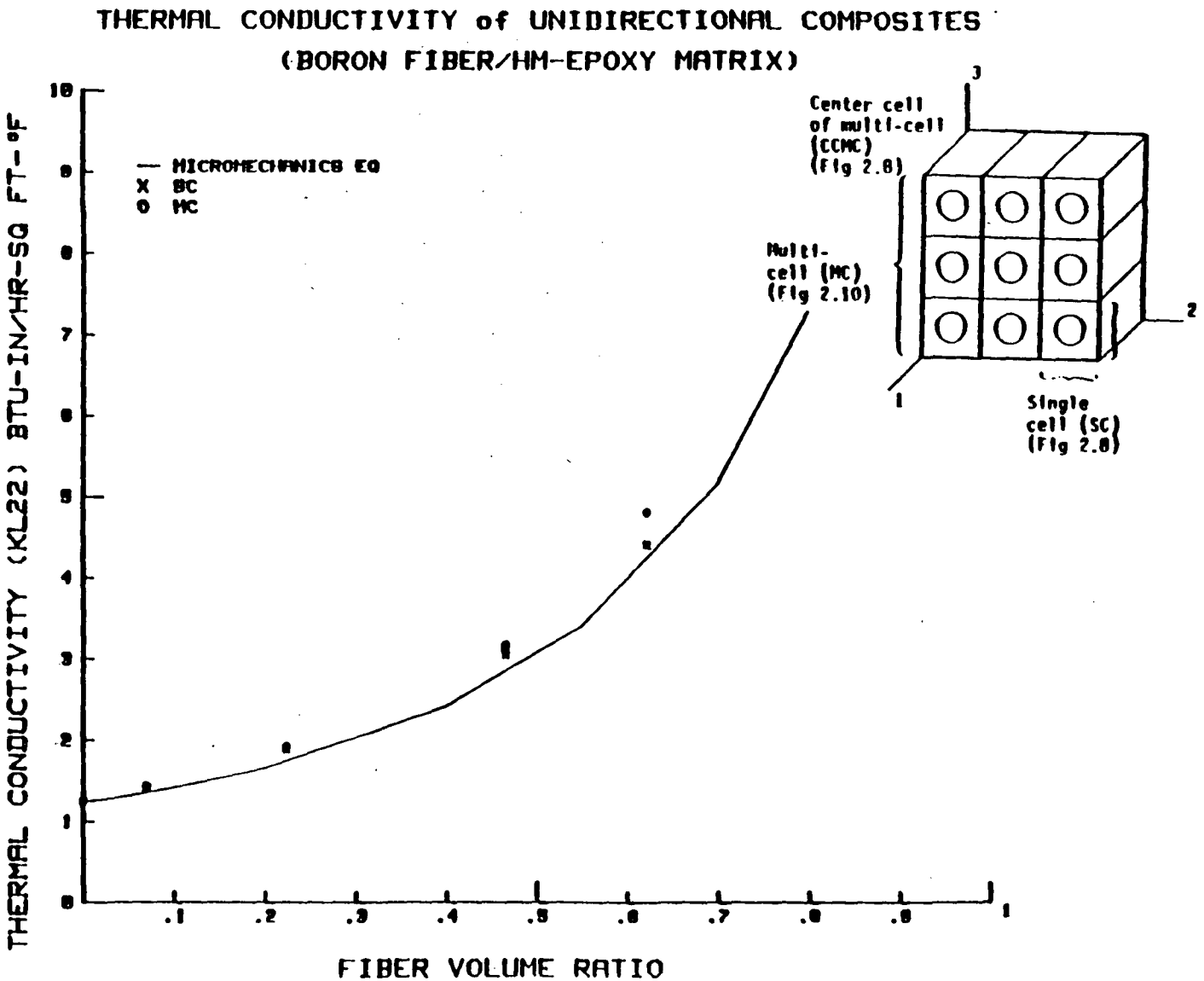
THERMAL CONDUCTIVITY of UNIDIRECTIONAL COMPOSITES
(BORON FIBER/HM-EPOXY MATRIX)
THERMAL CONDUCTIVITY (KL22) BTU-IN/HR-SQ FT-°F
FIBER VOLUME RATIO
— MICROMECHANICS EQ
X BC
o MC
Center cell of multi-cell (CCMC) (Fig 2.8)
Multi-cell (MC) (Fig 2.10)
Single cell (SC) (Fig 2.8)
1
2
3

Figure 3.10

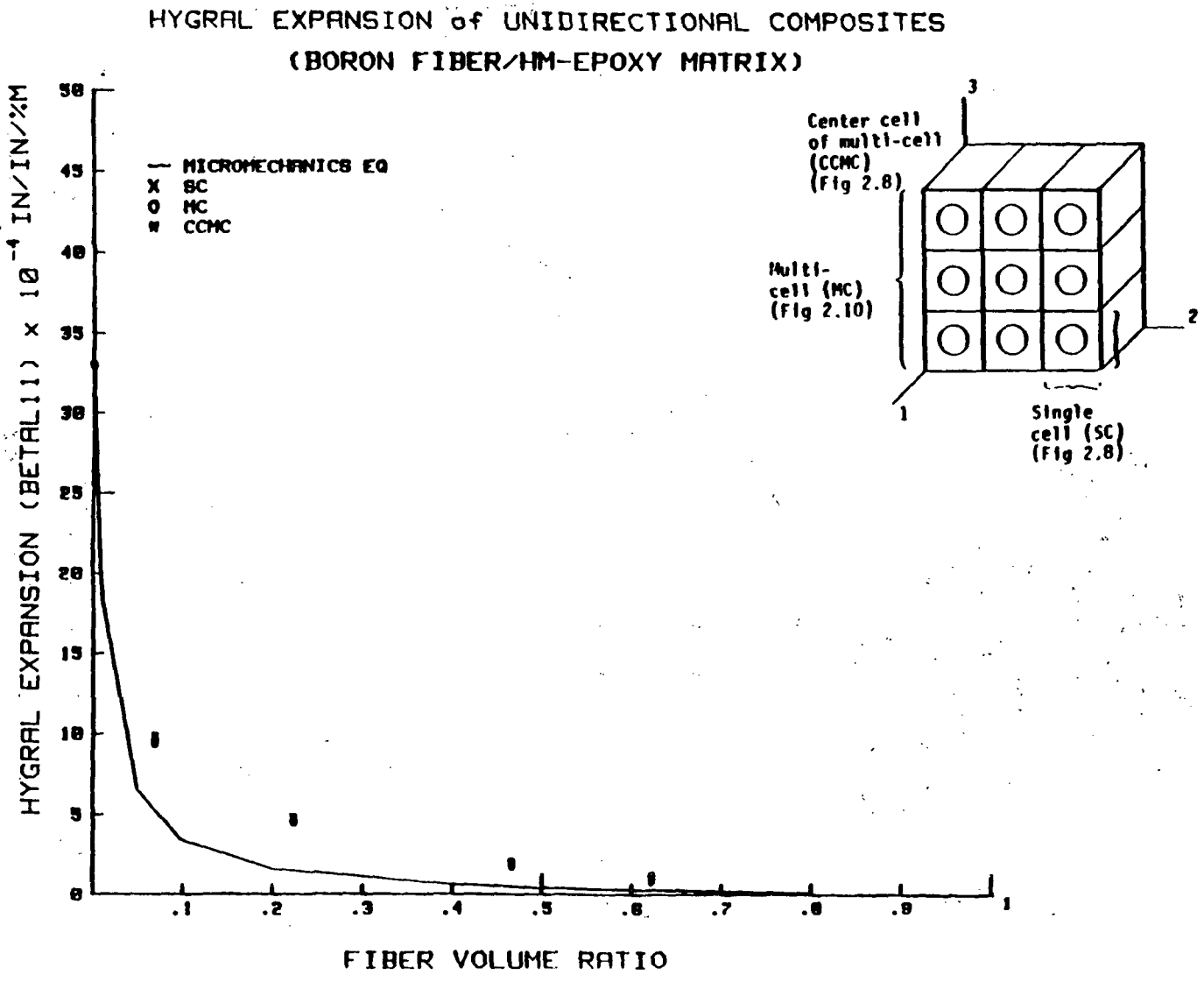
HYGRAL EXPANSION of UNIDIRECTIONAL COMPOSITES
(BORON FIBER/HM-EPOXY MATRIX)
HYGRAL EXPANSION (BETAL11) x 10⁻⁴ IN/IN/%M
— MICROMECHANICS EQ
X SC
O MC
■ CCMC
0
5
10
15
20
25
30
35
40
45
50
.1
.2
.3
.4
.5
.6
.7
.8
.9
1
FIBER VOLUME RATIO
Center cell of multi-cell (CCMC) (Fig 2.8)
Multi-cell (MC) (Fig 2.10)
Single cell (SC) (Fig 2.8)
1
2
3

Figure 3.11

TABLE 3.7

COMPARISON OF HYGRAL PROPERTIES OF UNIDIRECTIONAL COMPOSITES

		BORON/HM-EPOXY				S-GLASS/IMHS-EPOXY				AS/IMHS-EPOXY			
		u in/in%M		n in^2/sec		u in/in%M		n in^2/sec		u in/in%M		n in^2/sec	
CALC.	k_f	B_{L11}	B_{L22}	D_{L11}	D_{L22}	B_{L11}	B_{L22}	D_{L11}	D_{L22}	B_{L11}	B_{L22}	D_{L11}	D_{L22}
SC	.622	.100	1.48	.227	.145	.161	1.47	.227	.145	.121	1.57	.227	.145
MC		.082	1.31	.227	.147	.145	1.36	.227	.147	.098	1.47	.227	.147
CCMC		.120	1.22	--	--	.181	1.24	--	--	.131	1.43	--	--
SME		.026	.720	.227	.127	.079	.731	.227	.127	.032	.752	.227	.127
SC	.466	.203	2.08	.321	.220	.304	2.16	.321	.220	.233	2.18	.321	.220
MC		.173	1.99	.320	.228	.277	1.97	.320	.228	.200	2.13	.320	.228
CCMC		.206	1.94	--	--	.304	1.93	--	--	.229	2.09	--	--
SME		.048	1.14	.320	.190	.146	1.15	.320	.190	.060	1.18	.320	.190
SC	.224	.483	3.06	.466	.383	.764	3.01	.466	.383	.534	3.13	.466	.383
MC		.446	3.03	.466	.386	.682	2.97	.466	.386	.469	3.11	.466	.386
CCMC		.453	3.03	--	--	.680	2.97	--	--	.500	3.12	--	--
SME		.142	2.05	.466	.316	.405	2.05	.466	.316	.175	2.08	.466	.316
SC	.069	.986	3.64	.558	.519	1.49	3.50	.558	.519	1.08	3.66	.558	.519
MC		.961	3.58	.558	.525	1.46	3.50	.558	.525	1.06	3.66	.558	.525
CCMC		.932	3.66	--	--	1.44	3.52	--	--	1.02	3.67	--	--
SME		.488	2.86	.558	.442	1.16	2.86	.558	.442	.587	2.87	.558	.442

NOTES: SC = Single Cell; MC = Multi-Cell; CCMC = Center Cell of Multi-Cell;
SME = Simplified Micromechanics Equations

3.2.3.2. Transverse Hygral Coefficient of Expansion (B_{L22}). The procedure used to determine the transverse HEC is the same as that described for the longitudinal TEC.

The transverse HEC predicted from the SME is in poor agreement with the values predicted from the FE analysis as shown for boron/HM-epoxy in Figure 3.12. The three FE models predict different values for B_{L22} especially as k_f increases. The comparisons for the three composite systems are in Table 3.7. The same factors influencing A_{L22} are thought to affect the B_{L22} predictions as well.

3.2.3.3. Longitudinal Diffusivity (D_{L11}). The procedure used to analyze the longitudinal diffusivity is the same as that described for the longitudinal thermal conductivity except that the moisture diffusivity for the fibers are assumed to be zero.

The longitudinal diffusivity computed by the SME is in good agreement with the FE predictions as shown for the boron/HM-epoxy composite system in Figure 3.13. The three composite systems analyzed are summarized in Table 3.7.

3.2.3.4. Transverse Diffusivity (D_{L22}). The procedure used to analyze the transverse diffusivity is the same as that described for the transverse thermal conductivity except that the fiber diffusivity is assumed to be zero.

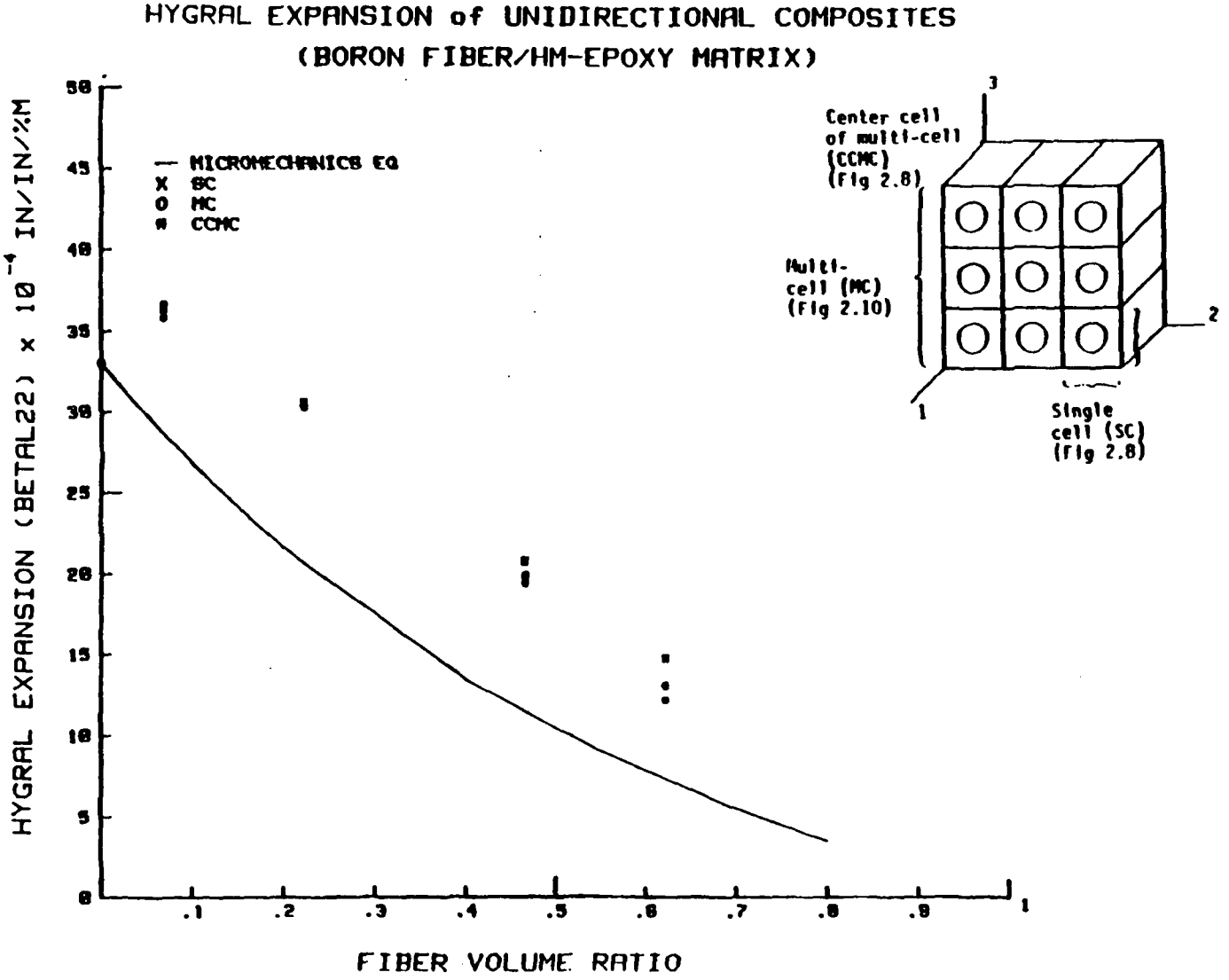
HYGRAL EXPANSION of UNIDIRECTIONAL COMPOSITES
(BORON FIBER/HM-EPOXY MATRIX)
HYGRAL EXPANSION (BETAL22) x 10⁻⁴ IN/IN/%M
— MICROMECHANICS EQ
X SC
O MC
* CCMC
FIBER VOLUME RATIO
Center cell of multi-cell (CCMC) (Fig 2.8)
Multi-cell (MC) (Fig 2.10)
Single cell (SC) (Fig 2.8)
1
2
3

Figure 3.12

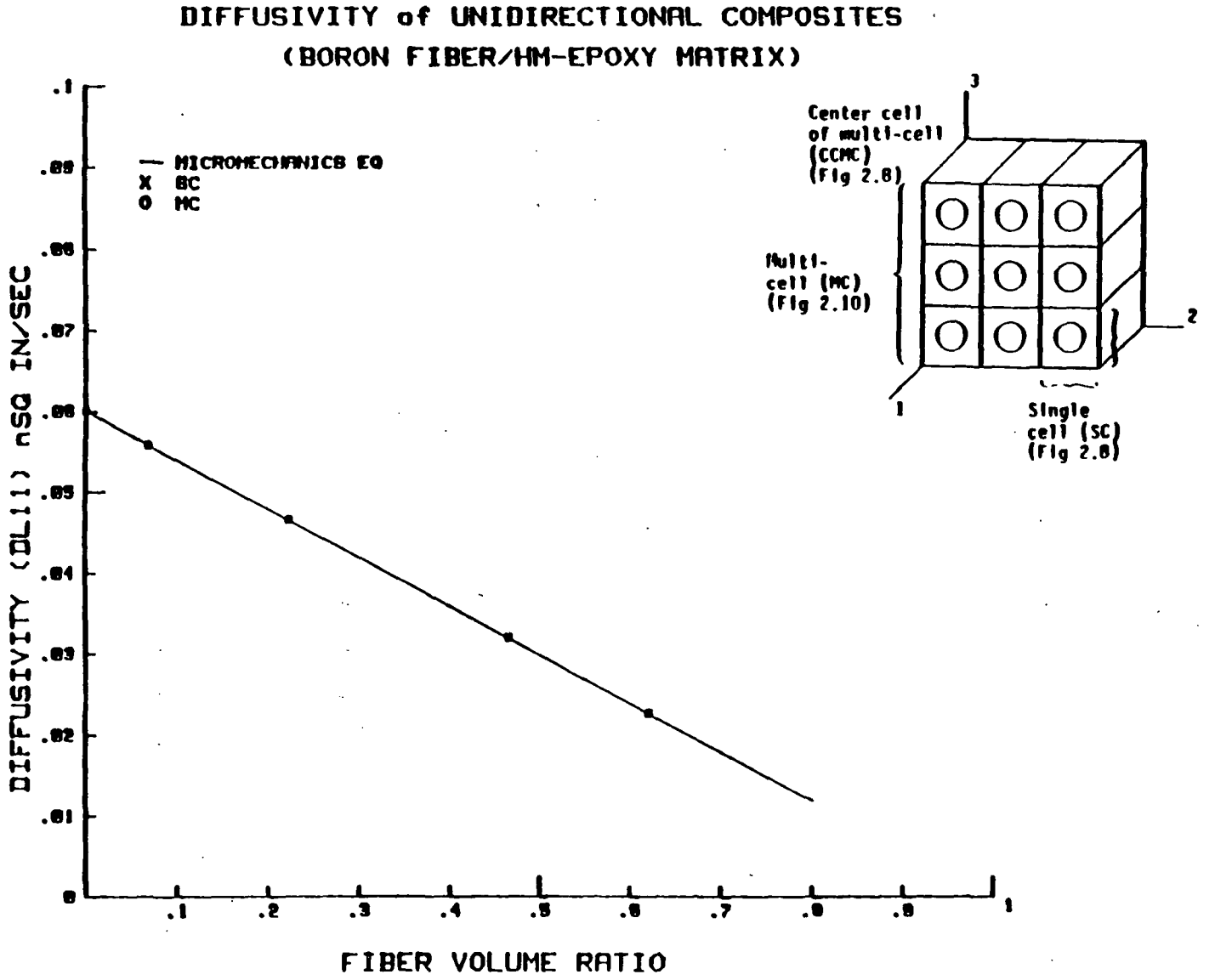
DIFFUSIVITY of UNIDIRECTIONAL COMPOSITES
(BORON FIBER/HM-EPOXY MATRIX)
— MICROMECHANICS EQ
X BC
O MC
DIFFUSIVITY (DL11) nSQ IN/SEC
.1
.09
.08
.07
.06
.05
.04
.03
.02
.01
0
.1
.2
.3
.4
.5
.6
.7
.8
.9
1
FIBER VOLUME RATIO
3
Center cell
of multi-cell
(CCMC)
(Fig 2.8)
Multi-
cell (MC)
(Fig 2.10)
2
1
Single
cell (SC)
(Fig 2.8)

Figure 3.13

The differences between the SME and the FE predictions are shown in Figure 3.14 for the boron/HM-epoxy composite system. Table 3.7 illustrates these differences for the three composite systems analyzed. Collectively these differences are acceptable in view of the approximations associated with the SME. The predictions from the three FE models are nearly identical.

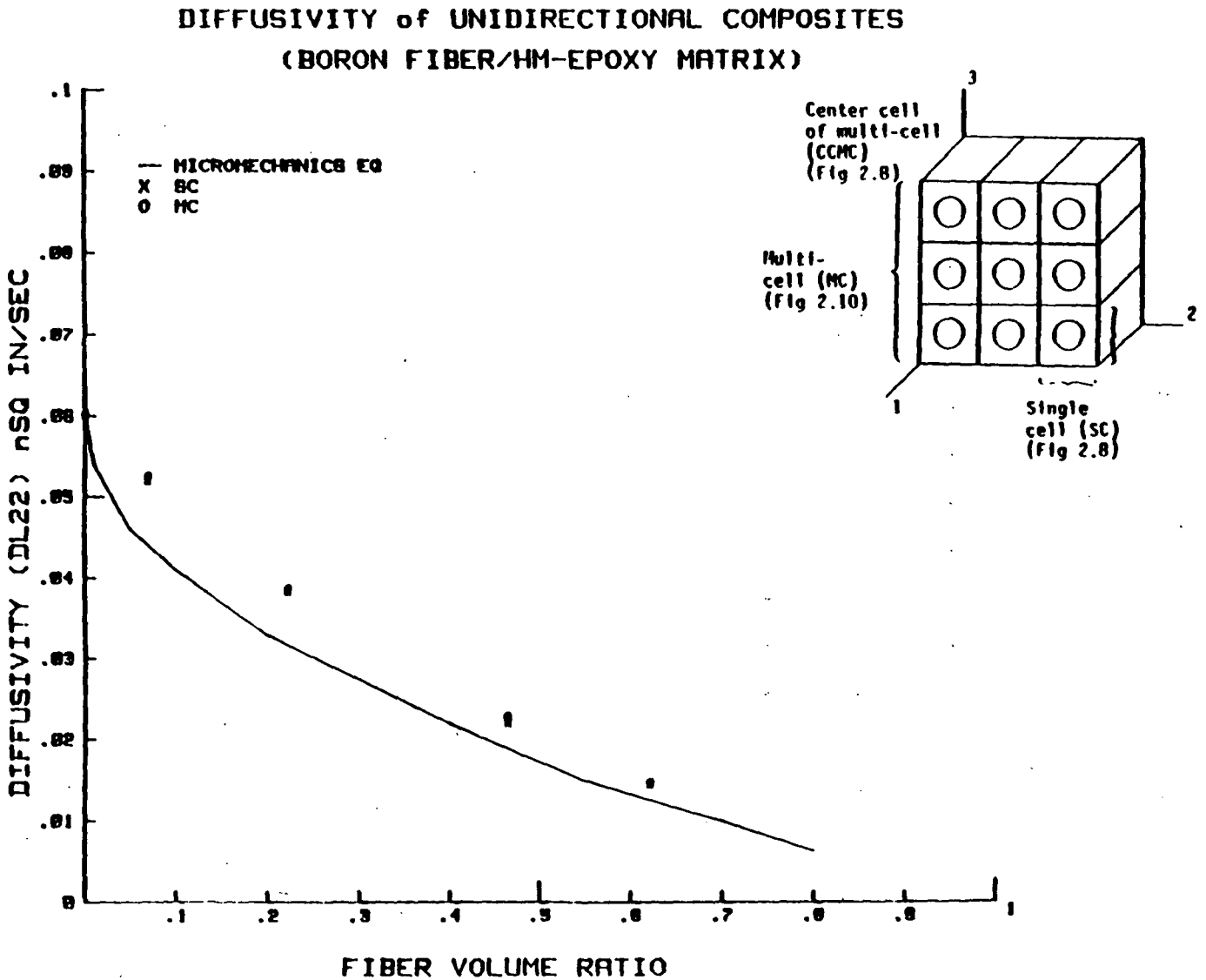
DIFFUSIVITY of UNIDIRECTIONAL COMPOSITES
(BORON FIBER/HM-EPOXY MATRIX)
— MICROMECHANICS EQ
X SC
O MC
DIFFUSIVITY (DL22) nSQ IN/SEC
.1
.09
.08
.07
.06
.05
.04
.03
.02
.01
0
.1
.2
.3
.4
.5
.6
.7
.8
.9
1
FIBER VOLUME RATIO
Center cell
of multi-cell
(CCMC)
(Fig 2.8)
Multi-
cell (MC)
(Fig 2.10)
Single
cell (SC)
(Fig 2.8)
3
2
1

Figure 3.14

CHAPTER 4

SUMMARY

4.1 Conclusions

The finite element (FE) investigation performed with the single cell (SC) model provides adequate values for the majority of the HTM properties (except GL23 and VL23) as compared with the multi-cell model (MC). The SC model provides accurate results for all composite systems using isotropic fiber (boron and s-glass) and isotropic matrix. The SC model also provides accurate results for composite systems using orthotropic fiber and isotropic matrix for the HTM properties as stated above.

The FE investigation using the MC model provides valuable information for composite property predictions. It first validates the SC model for the properties as described above. It also provides better results for VL23 that could not be obtained from the SC model because of boundary effects as well as effects due to the interaction between neighboring fibers. The MC model can also be used in a superelement analysis to better represent the ply.

The use of FE 3-D analysis provides insight into the use of the SME. The resulting comparisons between SME and FE predictions generally indicate good correlation except for GL23. It is thought at this time that the SME prediction for GL23 are more realistic than the FE predictions in view of the difficulties associated

with simulating the respective boundary conditions. Also the single cell FE model is adequate where the interaction effects from neighboring fibers are negligible. Furthermore, a 9-cell multi-cell model appears to be adequate for fiber composite micromechanics investigations assuming linear behavior. Finally, advanced FE methods, such as substructuring, can be applied to composite micromechanics in order to simulate a large number of individual fibers. The number of fibers included in the simulation by substructuring may be restricted by the CPU cost.

4.2 Recommendations

The superelement technique used for this investigation provides a number of options for future work. The first should be to perform a microstress analysis for the SC and MC models. The second should be to model and analyze a composite laminate for properties and stresses. The substructuring technique can be used to model and analyze composite laminate with inherent defects, voids, random fiber orientation, moisture pockets, etc. The limits of this technique are only that of practical structures and computer time.

REFERENCES

1. C. C. Chamis and G. P. Sendeckyj, "Critique on Theories Predicting Thermoelastic Properties of Fibrous Composites", J. Composites Mater., Vol. 2, No. 3, 1968, pp. 332-358.

2. J. F. Stevenson, "Discrete-Element Microstress Analysis of Unidirectional Fiber Composites", University Microfilms, Ann Arbor, 1970.

3. B. W. Rosen, "Thermal Expansion Coefficient of Composite Materials", Ann Arbor, 1968.

4. Lt. S. Han and M. Bashizadeh-Fakhar, "Transient Heat Flow Across Unidirectional Fibers in Composites", AFWAL-TR-83-3018.

5. C. C. Chamis, "Simplified Composite Micromechanics Equations for Hygral, Thermal and Mechanical Properties", NASA TM-83320, National Aeronautics and Space Administration, Washington, DC, 1983.

6. H. G. Schaeffer, "MSC/NASTRAN PRIMER: Static and Normal Modes Analysis", Schaeffer Analysis, New Hampshire, 1979.

7. E. P. Popov, "Mechanics of Materials", Prentice-Hall, New Jersey, 1976.

Page Intentionally Left Blank

APPENDIX: SAMPLE CALCULATIONS

The following calculations include those necessary for obtaining the hygral-thermal-mechanical (HTM) properties for the finite element models. All the HTM properties are included for the SC and MC predictions; however, the predictions for CCMC do not include the thermal conductivities and the diffusivities.

Single Cell Predictions

The following calculations show the steps used to compute the various composite material properties from the FE analysis results using the 192 element model.

Case 1 Static Equivalent Axial Displacement

From NASTRAN output, determine the total force on the surface at X=0 due to a uniform displacement applied to the surface at X=a (Fig 2.7). Compute the longitudinal Young's modulus (E_{L11}) from:

$$E_{L11} = (F \times X)/(A \times u) .$$

Where u = .0006 in., X = .060 in., A = 1.5725 $\times 10^{-4}$ sq. in. and F = 57.2 lb. (as determined from the single point constraint forces). Substituting these values into the equation, E_{L11} = 36.4 Mpsi.

From NASTRAN output, determine the average v-displacement on surface (Y=b) Fig 2.7. With this value compute Poisson's ratio

(V_{L12}) from:

$$V_{L12} = e_y/e_x \ , \ e_x = u/X \ , \ e_y = v/Y \ .$$

Where X = .060 in., Y = .01254 in., u = .0006 in. and $v = 3.15 \times 10^{-5}$in (as determined from grid point displacements). Substituting these values into the equations $V_{L12} = .251$.

Case 2 Uniform Hygral (Moisture) Load

From NASTRAN output, determine the average u-displacement of surface (X=a) Fig. 2.7. With this value, compute the longitudinal coefficient of hygral (moisture) expansion from:

$$B_{L11} = u/(M \times X) \ .$$

Where M = 100%, X = .03 in. and $u = 3.02 \times 10^{-4}$ in. Since the model is restrained at the center surface (X=a/2), the displacement of surface (X=a) represent only half of the total expansion (Fig. 2.7). To compensate for this in the above predictions, half of the total length (X = .06 in) is used. Substituting these values into the equation results in $B_{L11} = 1.0 \times 10^{-4}$ in/in/%M.

From NASTRAN output, determine the average v-displacement of surface (Y=b), Fig. 2.7. With this value, compute the transverse coefficient of hygral expansion from:

$$B_{L22} = v/(M \times Y) \ .$$

Where M = 100%, Y = .00627 in., $v = 9.25 \times 10^{-4}$in. Substitute these values into the equation results in $B_{L22} = 14.8 \times 10^{-4}$ in/in/%M.

Case 3 Uniform Temperature Load

From NASTRAN output, determine the average u-displacement of surface (X=a), Fig. 2.7. With this value, compute the longitudinal

coefficient of thermal expansion coefficient from:

$$A_{L11} = u/(T \times X) \ .$$

Where T = 1000°F, X = .03 in. and u = 1.18×10^{-4}in. Substituting these values into the equation, $A_{L11} = 3.93 \times 10^{-6}$ in/in-°F.

From NASTRAN output, determine the average v-displacement of surface (Y=b), Fig. 2.7. With this value, compute the transverse coefficient of thermal expansion from

$$A_{L22} = v/(T \times Y) \ .$$

Where T = 1000°F, Y = .00627 in. and v = 1.22×10^{-4}in. Substituting these values into the equation,

$A_{L22} = 19.4 \times 10^{-6}$ in/in-°F.

Case 4 Static Equivalent Transverse Displacement

From NASTRAN output, determine the total force on surface (Z=c), Fig. 2.7. With this value, compute the transverse modulus from:

$$E_{L22} = (F \times Z)/(A \times w) \ .$$

Where w = .00012 in., Z = .01254 in., A = 1.5048×10^{-4} sq. in. and F = 6.27 lb. Substituting these values into the equation yields E_{L22} = 4.35 Mpsi.

From NASTRAN output, determine the average v-displacement on surface (Y=b), Fig. 2.7. With this value, compute the Poisson's ratio from:

$$V_{L23} = e_y/e_z \ , \ e_y = v/Y \ , \ e_z = w/Z \ .$$

Where Z = .01254 in., Y = .01254 in., w = .0012 in. and v = 4.96×10^{-5}in. Substituting these values into the equation yields V_{L23} = .413 .

Case 5 Static Equivalent XY-Shear Displacement

From NASTRAN output, determine the total force on surface (Y=b), Fig. 2.7. With this value, compute the shear modulus from:

$$G_{L12} = T/g \ , \ g = u/Y \ , \ T = F/A \ .$$

Where u = .00012 in., Y = .01254 in., A = 1.5048×10^{-4} sq.in. and F = 1.94 lb. Substituting these values into the equation resulting in G_{L12} = 1.35 Mpsi.

Case 6 Static Equivalent YZ-Shear Displacement

From NASTRAN output, determine the total force in the z-direction on surface (Y=b), Fig. 2.7. With this value, compute the shear modulus from:

$$G_{L23} = T/g \ , \ g = w/Y \ , \ T = F/A \ .$$

Where w = .00012 in., Y = .01254 in., A = 1.5048×10^{-4} sq.in. and F = 2.14 lb. Substituting these values into the equation, G_{L23} = 1.49 Mpsi.

Case 7 Static Equivalent Longitudinal Heat Transfer

From NASTRAN output, determine the total flux on surface (X=a), Fig. 2.7. With this value, compute the thermal conductivity from:

$$K_{L11} = (Q_T/A)x(X/T) \ .$$

Where A = 1.5725×10^{-4} sq.in., X = .075 in., Q_T = 1.35 BTU-sq.in./hr-sq.ft. and T = 46 ^{o}F. Substituting these values into the equation, K_{L11} = 14.0 BTU-in./hr.-^{o}F-sq.ft.

Case 8 Static Equivalent Transverse Heat Transfer

From NASTRAN output, determine the total flux on surface (Y=b),

Fig. 2.7. With this value, compute the thermal conductivity from:

$$K_{L22} = (Q_T/A)x(Y/T) .$$

Where A = 1.5048×10^{-4} sq.in., Y = .01254 in., Q_T = 1.57 \ BTU-sq.in./hr.-sq.ft. and T = 30^{o}F. Substituting these values into the equation, K_{L22} = 4.41 BTU-in./hr.-^{o}F-sq.ft.

Case 9 Static Equivalent Longitudinal Hygral Transfer

From NASTRAN output, determine the total flux on surface (X=a), Fig. 2.7. With this value, compute the diffusivity from:

$$D_{L11} = (Q_M/A)x(X/T) .$$

Where A = 1.5725×10^{-4} sq.in., X = 0.3 in., $Q_M = 1.19 \times 10^{-11}$ and M = 999. Substituting these values into the equation yields $D_{L11} = 2.27 \times 10^{-11}$ sq.in./sec.

Case 10 Static Equivalent Transfer Hygral Transfer

From NASTRAN output, determine the total flux on surface (Y=b), Fig. 2.7. With this value, compute the diffusivity from:

$$D_{L22} = (Q_T/A)x(Y/T) .$$

Where A = 1.5048×10^{-4} sq.in., Y = .01254 in., $Q_M = .124 \times 10^{-11}$ and M = 7. Substituting these values into the equation results in $D_{L22} = 1.45 \times 10^{-11}$ sq.in./sec.

Multi-Cell Predictions

The following calculations indicate the process used to compute the material properties for the MC predictions.

Case 1 Static Equivalent Axial Displacement

From NASTRAN output, determine the total force on surface (X=0),

due to a uniform displacement applied to surface (X=a), Fig. 2.8. Compute the longitudinal Young's modulus (E_{L11}) from:

$$E_{L11} = (F \times X)/(A \times u) .$$

Where u = .0006 in., X = .060 in., A = 1.415×10^{-3} sq.in. and F = 515 lb. Substituting these values into the equation, E_{L11} = 36.4 Mpsi.

From NASTRAN output, determine the average v-displacement on surface (Y=b), Fig. 2.8. With this value, compute Poisson's ratio (V_{L12}) from:

$$V_{L12} = e_y/e_x \ , \ e_x = u/X \ , \ e_y = v/Y .$$

Where X = .060 in., Y = .03762 in., u = .0006 in. and v = 9.23×10^{-5}in. Substituting these values into the equations yields V_{L12} = .245 .

Case 2 Uniform Hygral Load

From NASTRAN output, determine the average u-displacement on surface (Y=b), Fig. 2.8. With this value, compute the longitudinal coefficient of hygral expansion from:

$$B_{L11} = u/(M \times X) .$$

Where M = 100%, X = .03 in., and u = 2.47×10^{-4}in. Substituting these values into the equation, B_{L11} = $.823 \times 10^{-4}$in/in-%M.

From NASTRAN output, determine the average v-displacement of surface (Y=b), Fig. 2.8. With this value, compute the transverse coefficient of hygral expansion from:

$$B_{L22} = v/(M \times Y) .$$

Where M = 100%, Y = .01881 in. and v = 2.47×10^{-3}in. Substituting these values into the equation, B_{L22} = 13.1×10^{-4} in/in-%M.

Case 3 Uniform Temperature Load

From NASTRAN output, determine the average u-displacement of surface (X=a), Fig. 2.8. With this value, determine the longitudinal coefficient of thermal expansion from:

$$A_{L11} = u/(T \times X) .$$

Where $T = 1000^{o}F$, $X = .03$ in. and $u = 1.12 \times 10^{-4}$in. Substituting these values into the equation, $A_{L11} = 3.73 \times 10^{-6}$ in/in-^{o}F.

From NASTRAN output, determine the average v-displacement on surface (Y=b), Fig. 2.8. With this value, compute the transverse coefficient of thermal expansion from:

$$A_{L22} = v/(T \times Y) .$$

Where $T = 1000^{o}F$, $Y = .01881$ in. and $v = 3.34 \times 10^{-4}$in. Substituting these values into the equation,

$A_{L22} = 17.8 \times 10^{-6}$ in/in-^{o}F.

Case 4 Static Equivalent Transverse Displacement

From NASTRAN output, determine the total force on surface (Z=c), Fig. 2.8. With this value, compute the transverse modulus (E_{L22}) from:

$$E_{L22} = (F \times Z)/(A \times w) .$$

Where $w = .00012$ in., $Z = .03762$ in., $A = 4.51 \times 10^{-4}$ sq.in. and $F = 6.62$ lb. Substituting these values into the equation yields $E_{L22} = 4.60$ Mpsi.

From NASTRAN output, determine the average y-translation as shown for V_{L12}. With this value, compute the Poisson's ratio

(V_{L23}) from:

$$V_{L23} = e_y/e_z \ , \ e_y = v/Y \ , \ e_z = w/Z \ .$$

Where w = .00012 in., Z = .03762 in., A = 4.51×10^{-4} sq. in. and Y = .03762 in. Substituting these values into the equation yields $V_{L23} = .212$.

Case 5 Static Equivalent XY-Shear Displacement

From NASTRAN output, determine the total force in the x-direction on surface (Y=b), Fig. 2.8. With this value, compute the shear modulus (G_{L12}) from:

$$G_{L12} = T/g \ , \ g = u/Y \ , \ T = F/A \ .$$

Where u = .00012 in., Y = .03752 in., A = 4.51×10^{-4} sq.in. and F = 1.94 lb. Substituting these values into the equation, $G_{L12} = 1.35$ Mpsi.

Case 6 Static Equivalent YZ-Shear Displacement

From NASTRAN output, determine the total force in the z-direction on surface (Y=b), Fig. 2.8. With this value, compute the shear modulus (G_{L23}) from:

$$G_{L23} = T/g \ , \ g = w/Y \ , \ T = F/A \ .$$

Where w = .00012 in., Y = .03762 in., A = 4.51×10^{-4} sq.in. and F = 2.15 lb. Substituting these values into the equation, $G_{L23} = 1.49$ Mpsi.

Case 7 Static Equivalent Longitudinal Heat Transfer

From NASTRAN output, determine the total flux on surface (X=a), Fig. 2.7. With this value, compute the thermal conductivity from:

$$K_{L11} = (Q_T/A)x(X/T) \ .$$

Where A = 1.415×10^{-3} sq.in., X = .075 in., Q_T = 12.26 BTU-sq.in./hr.-sq.ft. and T = 46 ^{o}F. Substituting these values into the equation, K_{L11} = 14.2 BTU-in./hr-sq.ft.-^{o}F.

Case 8 Static Equivalent Transverse Heat Transfer

From NASTRAN output, determine the total flux on surface (Y=b) Fig. 2.8. With this value, compute the transverse thermal conductivity from:

$$K_{L22} = (Q_T/A)x(Y/T) .$$

Where A = 4.51×10^{-4} sq.in., X = .03762 in., Q_T = 4.46 BTU-sq.ins/hr-sq.ft.-^{o}F and T = 78 F. Substituting these values into the equation, K_{L22} = 4.80 BTU-in/hr-sq.ft.-^{o}F.

Case 9 Static Equivalent Longitudinal Hygral Transfer

From NASTRAN output, determine the total flux on surface (X=a) Fig. 2.8. With this value, compute the longitudinal diffusivity from:

$$D_{L11} = (Q_M/A)x(X/M) .$$

Where A = 4.51×10^{-4} sq.in., X = .012 in., $Q_M = 2.67 \times 10^{-9}$ and M = 999.0. Substituting these values into the equation results in $D_{L11} = 2.27 \times 10^{-11}$ sq.in./sec.

Case 10 Static Equivalent Transverse Hygral Transfer

From NASTRAN output, determine the total flux on surface (X=a), Fig. 2.8. With this value, compute the transverse diffusivity from:

$$D_{L22} = (Q_M/A)x(Y/T) .$$

Where A = 4.51×10^{-4} sq.in., Y = .03762., $Q_M = 3.67 \times 10^{-12}$ and M = 21.0. Substituting these values into the equation results in $D_{L22} = 1.47 \times 10^{-11}$ sq.in./sec.

Center Cell of the Multi-Cell Predictions

The following calculations indicate the process used to compute the material properties for the CCMC calculations.

Case 1 Static Equivalent Axial Displacement

From NASTRAN output, determine the total force on surface (X=0) due to a uniform displacement applied to surface (X=a). Compute the longitudinal modulus (E_{L11}) from:

$$E_{L11} = (F \times X)/(A \times u) .$$

Where $u = .0006$ in., $X = .06$ in., $A = 1.5725 \times 10^{-4}$ sq.in. and $F = 57.6$ lb. Substituting these values into the equation, $E_{L11} = 36.6$ Mpsi.

From NASTRAN output, determine the average v-displacement on surface(Y=2b/3) Fig 2.8. With this value, compute Poisson's ratio (V_{L12}) from:

$$V_{L12} = e_y/e_x \ , \ e_x = u/X \ , \ e_y = v/Y .$$

Where $X = .06$ in., $Y = .01254$ in., $u = .0006$ in. and $v = 3.03 \times 10^{-5}$ in. Substituting these values into the equation, $V_{L12} = .242$.

Case 2 Uniform Hygral Load

From NASTRAN output, determine the average u-displacement of surface(X=a) Fig 2.8 due to a uniform moisture absorption. With this value, compute the longitudinal coefficient of hygral expansion from:

$$B_{L11} = u/(M \times X) .$$

Where $M = 100\%$, $X = .03$ in. and $u = 3.61 \times 10^{-4}$ in. Substituting these values into the equation, $B_{L11} = 1.20 \times 10^{-4}$ in./in./%M.

From NASTRAN output, determine the average v-displacement of surface(Y=2b/3) Fig 2.8. With this value, compute the transverse coefficient of hygral expansion from:

$$B_{L22} = v/(M \times Y) .$$

Where M = 100% , X = .00627 in. and v = 7.67×10^{-4}in. Substituting these values into the equation, $B_{L22} = 12.2 \times 10^{-4}$ in./in./%M.

Case 3 Uniform Temperature Load

From NASTRAN output, determine the average u-displacement of surface(X=a) Fig 2.8 due to a uniform temperature. With this value, compute the longitudinal coefficient of thermal expansion from:

$$A_{L11} = u/(T \times X) .$$

Where T = 1000^{o}F X = .030 in. and u = 1.25×10^{-4} in. Substituting these values into the equation, $A_{L11} = 4.16 \times 10^{-6}$ in./in.-^{o}F

From NASTRAN output, determine the average v-displacement of surface (Y=2b/3) Fig 2.8. With this value, compute the transverse coefficient of thermal expansion from:

$$A_{L22} = v/(T \times Y) .$$

Where T = 1000^{o}F , Y = .00627 in. and v = 1.04×10^{-4}in. Substituting these values into the equation,

$A_{L22} = 16.6 \times 10^{-6}$ in./in.-^{o}f

Case 4 Static Equivalent Transverse Displacement

From NASTRAN output, determine the total force on surface (Z=2c/3)due to a displacement on surface (Z=0) Fig 2.8. With this value, compute the transverse modulus (E_{L22}) from:

$$E_{L22} = (F \times Z)/(A \times w) .$$

Where Z = .01254 in. , A = 4.51 x 10^{-4} sq.in., w = 4.0 x 10^{-4} in. and F = 66.2 lb. Substituting these values into the equation, E_{L22} = 4.60 Mpsi.

From NASTRAN output, determine the average v-displacement of surface (Y=2b/3) Fig 2.8. With this value, compute the Poisson's ratio (V_{L23}) from:

$$V_{L23} = e_y/e_z \ , \ e_y = v/Y \ , \ e_z = w/Z \ .$$

Where Z = .01254 , Y = .01254 in., v = 6.12 x 10^{-6} in. and w = 4.0 x 10^{-5} in. Substituting these values into the equation, V_{L23} = .153.

Case 5 Static Equivalent XY-Shear Displacement

From NASTRAN output, determine the total force in the x-direction on surface (X=a). With this value, compute the shear modulus (G_{L12}) from:

$$G_{L12} = T/g \ , \ g = u/Y \ , \ T = F/A \ .$$

Where Y = .01254 , A = 4.51 x 10^{-4} sq.in., u = 4.0 x 10^{-5} in. and F = 1.94 lb. Substituting these values into the equations, G_{L12} = 1.35 Mpsi.

Case 6 Static Equivalent YZ-Shear Displacement

From NASTRAN output, determine the total force in the z-direction on surface (Y=2b/3).. With this value, compute the shear modulus (G_{L23}) from:

$$G_{L23} = T/g \ , \ g = w/Y \ , \ T = F/A \ .$$

Where Y = .01254 , A = 4.51 sq.in., w = 4.0 x 10^{-5} in. and F = 2.14 lb. Substituting these values into the equations, G_{L23} =1.49 Mpsi.

1. Report No.	2. Government Accession No.	3. Recipient's Catalog No.
NASA TM-83729		

4. Title and Subtitle	5. Report Date
Application of Finite Element Substructuring to Composite Micromechanics	August 1984
	6. Performing Organization Code: 505-33-5B

7. Author(s)	8. Performing Organization Report No.
John J. Caruso	E-2203
	10. Work Unit No.

9. Performing Organization Name and Address	11. Contract or Grant No.
National Aeronautics and Space Administration Lewis Research Center Cleveland, Ohio 44135	13. Type of Report and Period Covered: Technical Memorandum

12. Sponsoring Agency Name and Address	14. Sponsoring Agency Code
National Aeronautics and Space Administration Washington, D.C. 20546	

15. Supplementary Notes

This report was submitted as a thesis in partial fulfillment of the requirements for the degree Master of Science in Civil Engineering to The University of Akron, Akron, Ohio in May 1984 (work funded through NASA grant NSG 3-50).

16. Abstract

Finite element substructuring is used to predict unidirectional fiber composite hygral (moisture), thermal, and mechanical properties. COSMIC NASTRAN and MSC/NASTRAN are used to perform the finite element analysis. The results obtained from the finite element model are compared with those obtained from the simplified composite micromechanics equations. A unidirectional composite structure made of boron/HM-epoxy, s-glass/IMHS-epoxy and AS/IMHS-epoxy are studied. The finite element analysis is performed using three dimensional isoparametric brick elements and two distinct models. The first model consists of a single cell (one fiber surrounded by matrix) to form a square. The second model uses the single cell and substructuring to form a nine cell square array. To compare computer time and results with the nine cell superelement model, another nine cell model is constructed using conventional mesh generation techniques. An independent computer program consisting of the simplified micromechanics equation is developed to predict the hygral, thermal, and mechanical properties for this comparison. The results indicate that advanced techniques can be used advantageously for fiber composite micromechanics.

17. Key Words (Suggested by Author(s))	18. Distribution Statement
Composites; Boron epoxy; S-glass epoxy; AS-graphite epoxy; Micromechanics equations; Finite element substructuring	Unclassified - unlimited STAR Category 24

19. Security Classif. (of this report)	20. Security Classif. (of this page)	21. No. of pages	22. Price*
Unclassified	Unclassified		

*For sale by the National Technical Information Service, Springfield, Virginia 22161

National Aeronautics and
Space Administration

Washington, D.C.
20546

Official Business
Penalty for Private Use, $300

SPECIAL FOURTH CLASS MAIL
BOOK

Postage and Fees Paid
National Aeronautics and
Space Administration
NASA-451

NASA

POSTMASTER: If Undeliverable (Section 158
Postal Manual) Do Not Return